

NIST Advanced Manufacturing Series 100-14

**Prediction of Solidification Phases in
Cr-Ni Stainless Steel Alloys
Manufactured by Laser Based Powder
Bed Fusion Process**

Gregor Jacob

This publication is available free of charge from:
<https://doi.org/10.6028/NIST.AMS.100-14>

NIST
National Institute of
Standards and Technology
U.S. Department of Commerce

NIST Advanced Manufacturing Series 100-14

**Prediction of Solidification Phases in
Cr-Ni Stainless Steel Alloys
Manufactured by Laser Based Powder
Bed Fusion Process**

Gregor Jacob*
*Engineering Laboratory,
National Institute of Standards and Technology,
Gaithersburg, MD 20899 USA*

**Currently with Citim GmbH, 39179 Barleben, Germany*

This publication is available free of charge from:
<https://doi.org/10.6028/NIST.AMS.100-14>

March 2018



U.S. Department of Commerce
Wilbur L. Ross, Jr., Secretary

National Institute of Standards and Technology
Walter Copan, NIST Director and Undersecretary of Commerce for Standards and Technology

Disclaimer

Certain commercial entities, equipment, or materials may be identified in this document in order to describe an experimental procedure or concept adequately. Such identification is not intended to imply recommendation or endorsement by the National Institute of Standards and Technology, nor is it intended to imply that the entities, materials, or equipment are necessarily the best available for the purpose.

Official contribution of the National Institute of Standards and Technology (NIST); not subject to copyright in the United States. The full descriptions of the procedures used in this paper require the identification of certain commercial products. The inclusion of such information should in no way be construed as indicating that such products are endorsed by NIST or are recommended by NIST or that they are necessarily the best materials, instruments, software or suppliers for the purposes described.

Abstract

The microstructure and strength of chromium-nickel (Cr-Ni) stainless steel alloy parts is highly dependent on the chemical composition of the material and the thermal cycling it experiences during each processing step. This is particularly true when utilizing a laser powder bed fusion (LPBF) process to create the part. LPBF is an additive manufacturing (AM) process that quickly scans a laser over thin layers of powder to melt and solidify the powder to create the part. This results in rapid heating and cooling of the material that is dependent on the processing conditions and part geometry. Consequently, it is necessary to understand how these heating and cooling rates affect the resulting material phases of the final part. Only then the manufacturer can have confidence that the part will perform as intended. The objective of the report is to provide LPBF users with the necessary background to develop processing conditions that will achieve their microstructural design objectives.

This report outlines the established methods, using chemical-composition-based phase diagrams (Schäffler and DeLong diagrams), to predict the material microstructure of stainless steel weld metals and applies those methods to LPBF manufactured Cr-Ni stainless steel (S17-4¹). Predictions of the solidification phases in Cr-Ni stainless steel alloys, based on the ratio of the Cr and Ni equivalent, are shown. Incorporating these ratios into the phase solidification diagram helps to predict whether the solidification of a Cr-Ni stainless steel occurs in primary ferritic or austenitic phase. This approach also helps users to understand how the increased nitrogen content in additively manufactured S17-4 results in the greater retention of austenite compared to the same material produced by traditional methods. These diagrams can also inform the users about the stability of the retained austenite and its likelihood to decompose into other phases, such as martensite and cementite. In addition to outlining how phase solidification diagrams can help AM users better understand the material they produce, this report also compares results from literature describing microstructure of LPBF fabricated S17-4 with the predicted microstructure before and after different heat treatments. The report also shows that the fine columnar austenitic-martensitic-ferritic microstructure of as-manufactured S17-4 has changed into a predominant martensitic microstructure by a cryogenic treatment, resulting in an increase of hardness.

Furthermore, results of mechanical property measurements on additively manufactured S17-4 from other research work are compared and discussed in the result section to explain possibilities of the material phase transformations during different heat treatments, which lead to changes in the mechanical material properties.

Key words

Additive Manufacturing; Austenite; Cryogenic; DeLong Diagram; Equivalent chromium content; Heat treatment; Martensite; Nickel Equivalent; Powder Bed Fusion; Precipitation Hardening; Schäffler Diagram; Selective Laser Melting; Stainless Steel; Sub-zero.

¹ This material has the chemical composition corresponding to the stainless steel with official designation of UNS S17400. S17-4 implies precipitation hardening, which may or may not be the case for this powder. This shorthand designation is used in this paper following the customary usage in the AM field.

Table of Contents

Disclaimer	i
Abstract.....	ii
1. Introduction and background	1
1.1. Terminology	1
1.2. Crystal structure with associated elementary cell	1
1.3. Phases of metastable Fe-Fe ₃ C system	3
1.3.1. Partial systems in the Fe- Fe ₃ C diagram.....	4
1.4. Phase transformations during cooling.....	5
1.4.1. Martensite formation	6
1.4.2. Metallurgical characteristics of corrosion-resistant steel alloys manufactured by welding	8
1.4.3. Corrosion resistant Cr-Ni stainless steel alloys used in additive manufacturing applications.....	11
2. Prediction of microstructure transformation	11
2.1. Isothermal and continuous cooling microstructure prediction	11
2.2. The prediction of microstructure in welding applications.....	13
2.3. The inclusion of nitrogen in the microstructure prediction.....	14
2.4. Stability of retained austenite in the microstructure.....	16
3. Experimental validation: S17-4 manufactured by LPBF	18
4. Results and Discussion	20
5. Conclusions.....	26
Acknowledgments	28
References.....	28

List of Tables

Table 1. Terminology in a binary phase system.	1
Table 2. Schematic illustration of four crystal systems (BRAVIAS lattice) with associated elementary cell [4].	2
Table 3. Phases in Fe-Fe ₃ C system [7,8].....	4
Table 4. Correlation between cooling rates and obtained microstructure [9].....	6
Table 5. Chemical composition of the virgin stainless steels S17-4 and S15-5 powders as reported by the powder supplier [13, 14].....	8
Table 6. Computed Chromium-Equivalent (Cr _{Equ}) and Nickel-Equivalent (Ni _{Equ}) values for S17-4 and S15-5.....	13
Table 7. Calculated modified nickel-equivalents values; Ni _{Equ-mod} and Ni _{Equ-modCu} for S17-4 and S15-5 depending on the content of nitrogen and copper.....	15

Table 8. Computed M_{d30} for S17-4 and S15-5 depending on their N_2 content.....	17
Table 9. Nominal machine settings for this study.....	19

List of Figures

Fig. 1. Thermal analysis of pure iron [6].	3
Fig. 2. Binary phase diagram of Fe-C and Fe-Fe ₃ C system; with phase areas [8].	4
Fig. 3. Partial systems in metastable Fe-Fe ₃ C system [8].....	5
Fig. 4. Schematic martensite formation with forced solid solved carbon in BCT lattice structure [7]......	7
Fig. 5. Illustration of three phase solidification diagram [16].	9
Fig. 6. Microstructure obtained with different laser treatment parameters, a) longitudinal section of eutectic structure at $V_s = 1.7 \mu\text{m/s}$, b) cross section of a, c) stable δ - cells at $V_s = 400 \mu\text{m/s}$, and d) metastable γ - dendrites at $V_s = 1000 \mu\text{m/s}$ [25]......	10
Fig. 7. Isothermal TTT Diagram of a martensitic stainless steel type X39Cr13 (similar to AISI 420C) [28].	12
Fig. 8. Continuous Cooling Transformation (CCT) diagram, [10]......	12
Fig. 9. Possible microstructure of S17-4 and S15-5 according to the Schöffler Diagram [2], percentage of ferrite (% f).....	14
Fig. 10. Possible microstructure of S17-4 according to the Delong Diagram and equations for Cr_{Equ} , $Ni_{\text{Equ-mod}}$, and $Ni_{\text{Equ-modCu}}$, percentage of δ - ferrite (% δ -f).	15
Fig. 11. Possible microstructure of S15-5 according to the Delong Diagram and equations for Cr_{Equ} , $Ni_{\text{Equ-mod}}$, and $Ni_{\text{Equ-modCu}}$, percentage of δ - ferrite (% δ -f).	15
Fig. 12. Specimen arrangement on build platform, recoater direction parallel to Datum A moving from right to left. Dimensions are in mm.	19
Fig. 13. Specimen arrangement for the second study showing build plate (1), witness cubes (2), powder collection capsules (3) and tensile specimens (4) [51]......	19
Fig. 14. Tensile stress strain curves of PBF manufactured S17-4 in stress-relief heat treated condition; extensometer signal (A) and maximum strain (B) [51]......	21
Fig. 15. Microstructure of AM S17-4 steel using the virgin powder along the build direction at low magnification (A), and high magnification (B) [51]......	22
Fig. 16. Microstructure of S17-4 produced by LPBF, optical microscopy (left) and SEM (right) show strongly oriented, fine γ - grains [38]......	23
Fig. 17. SEM images (cross section view) of S17-4 manufactured by LPBF, a) overview, b) and c) magnified images from a, d) columnar grains parallel to building direction, e) columnar grain inclined to building direction, and f) columnar grain perpendicular to building direction, [54].	23
Fig. 18. SEM images in XY (a, b, and c) and YZ (d, e, and f) planes of S17-4 manufactured with various process parameters, [46].	24
Fig. 19. Results of hardness measurement (HRC scale) for S17-4 in three different conditions, error bars are one standard deviation.	25

1. Introduction and background

The examination of the material microstructure and mechanical properties for austenitic, ferritic, martensitic, and austenitic/martensitic stainless steels (e.g., Cr-Ni steel alloys) manufactured by laser based powder bed fusion (LPBF) processes has been the topic in many studies. All these studies investigated the effect of different process parameters on the manufactured specimen material. Conclusions regarding the effect of the chosen process parameters on the material microstructure could only be made after the specimen was manufactured and its material was examined.

This study focuses on the prediction of the microstructure of two different chromium (Cr)- nickel (Ni)- steel alloys (S17-4PH and S15-5 [1]) manufactured by LPBF processes. The use of the Schöffler and Delong Diagrams [2,3], which are established tools for the prediction of the microstructures of stainless steel weld metals, is assessed for this purpose. Microstructures of S17 4 and S15-5 are predicted using these tools by considering chemical contents and the thermal conditions during the LPBF process. Those predictions are compared with experimentally obtained microstructures of LPBF manufactured steel alloys reported by several previous studies. However, due to the several orders of magnitude difference in cooling rates of welding and LPBF processes, the predictions are qualitative in nature.

1.1. Terminology

Table 1 summarizes the commonly accepted terms and symbols for binary and ternary phase systems that will be used in this study.

Table 1. Terminology in a binary phase system.

Abbreviation	Description
Fe, C, Ni, Cr, ...	Pure elements, pure metals
S, L ...	Solid, Liquid
E (P, T, and B)	Eutectoid (Perlite, Troosite, Bainite)
Ec (L1 and L2)	Eutectic (Ledeburite I and Ledeburite II)
BCC, BCT, and FCC	Type of elementary cell
α , β , γ , δ , and ϵ	Solid solution
Fe_3C , M_{23}C_6 , ...	Stoichiometric phase (Intermediate, Intermetallic)
A_1 , A_2 , A_3 , ...	Transus temperature(s)

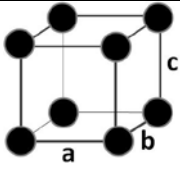
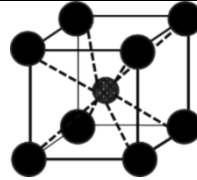
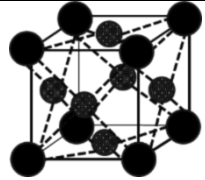
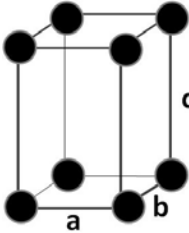
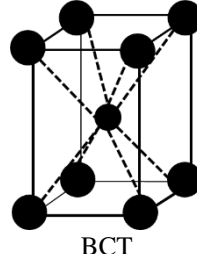
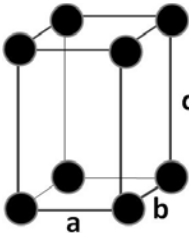
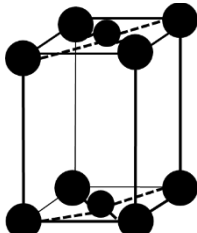
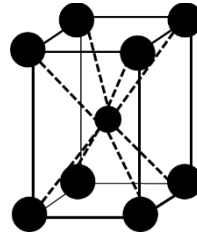
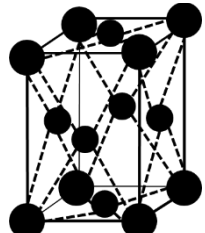
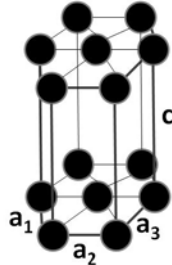
1.2. Crystal structure with associated elementary cell

A crystal is a homogeneous, three-dimensional solid body, whose atoms or molecules are arranged in a periodic order [4]. The smallest group of atoms/molecules that constitutes the repeating pattern is called the elementary (unit) cell of the crystal structure. A phase is a pure element or mixture of more than one element with uniform properties along the lattice depending on the crystal orientation. The border, where the properties change, is defined as a phase boundary. Phases in a microstructure can be different in their crystal orientation, crystal structure, and chemical composition. Table 2 shows only four of seven possible crystal systems with their possible types of elementary cells [4-7].

Pure metals, with a few exceptions, consist of cubic or hexagonal crystal systems. Tetragonal and rhombic systems may occur when inclusion elements distort the native cubic structure. Pure

metals can also exist in more than one crystal structure, also called crystal phases, and can go through phase changes depending on changing temperature, pressure, and chemical composition.

Table 2. Schematic illustration of four crystal systems (BRAVIAS lattice) with associated elementary cell [4].

Crystal system	Lattice constant	Type of Elementary cell (lattice structure)			
		Primitive	Simple base centric	Body centric (BC ₁)	Face centric (FC ₁)
Cubic (C)	$a = b = c$		Does Not exist	 BCC	 FCC
Tetragonal (T)	$a = b \neq c$		Does Not exist	 BCT	Does Not exist
Rhombic, orthorhombic	$a \neq b \neq c$				
Hexagonal	$a_1 = a_2 = a_3 \neq c$		Does Not exist	Does Not exist	Does Not exist

 atom of element

The phase transformation of pure metals and metal alloys can be determined by many different methods, including: thermodynamic analysis, in which phase transformation is detected through the analysis of enthalpy (differential scanning calorimetry and differential thermal analysis), and thermo-mechanical analysis (dilatometry), in which the phase transformation is detected by measuring the change in volume of the material. During continuous heating or cooling of a metal, phase changes will occur at certain temperatures. The phase transformation causes recalescence, which is the change in temperature due to the change in entropy. It is indicated as a discontinuity in a typical temperature versus time plot. For example, Fig. 1 shows the recalescence of pure iron as it cools and heats up as well as corresponding crystal phase changes. At room temperature and

normal pressure, iron solidifies in a body centered cubic (BCC) lattice structure (i.e., α -ferrite). At a higher, so called γ -transus temperature (A_3), the α -iron transforms into a face centered cubic (FCC) lattice structure, (i.e., γ -austenite). When reaching the temperature of 1392 °C the FCC γ -austenite transforms into BCC δ -ferrite. The smaller lattice constants of ferrite lead to a reduced capability to solve foreign elements like carbon in between the narrower arranged iron atoms.

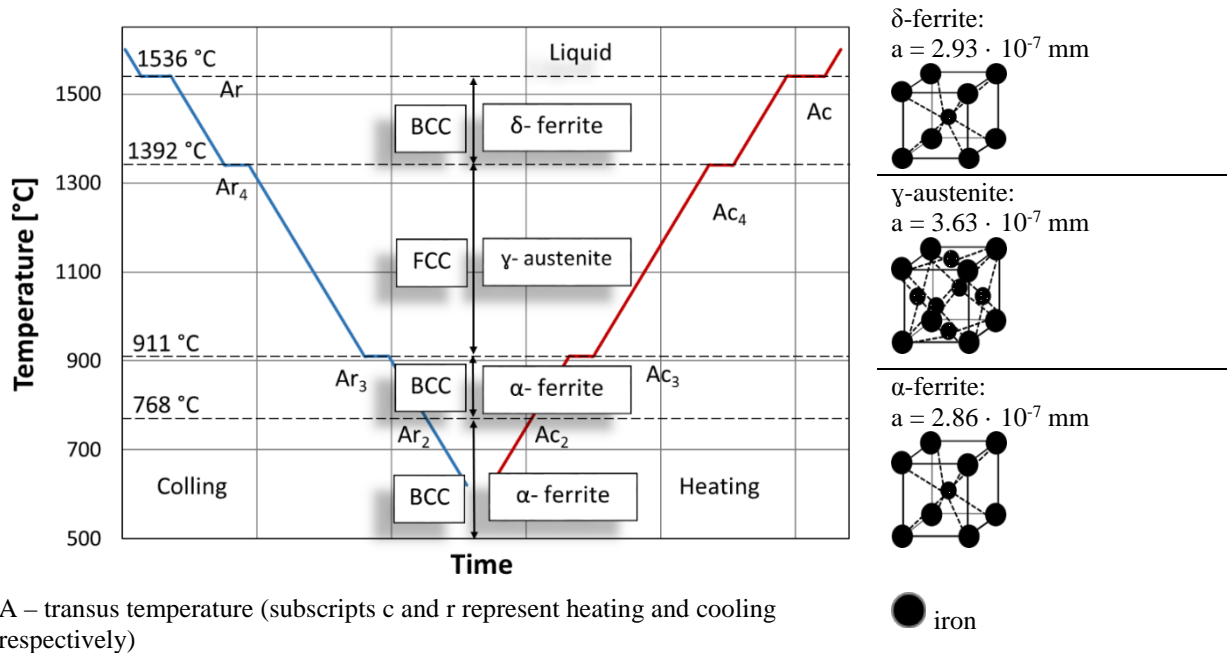


Fig. 1. Thermal analysis of pure iron [6].

An interesting phenomenon occurs at A_2 in Fig. 1. At the Curie temperature of 768 °C, the BCC orientation (α -ferrite) of the lattice structure does not change, but its magnetic behavior transitions from being ferromagnetic to paramagnetic.

1.3. Phases of metastable Fe-Fe₃C system

As carbon is added to iron to create steel, the amount dissolved into the iron lattice structure is dependent on temperature. When the amount of carbon reaches 6.68 wt%, then the material will turn into cementite (Fe₃C). Up to this point, depending on the temperature and the capacity of the lattice structure to dissolve carbon atoms, different amounts of iron phases are mixed with cementite. This is called as metastable Fe-Fe₃C system since the phases of the alloy change as a function of temperature and the carbon content. Table 3 lists the possible phases that can occur in the metastable Fe-Fe₃C system. The transformation between these phases (in equilibrium) as a function of temperature and carbon amount is illustrated in the binary Fe-C phase diagram shown in Fig. 2. The dotted lines in the binary Fe-C phase diagram indicate the stable Fe-C system.

Table 3. Phases in Fe-Fe₃C system [7,8].

Term	Phase	Transus Temperature ("A...")	Comment	Points and Lines
L	Liquid	A _L < 1536 °C		Line A-B-C-D
δ	Ferrite	A ₄ ; 1392 °C - 1536 °C	Solid solution	
α	Austenite	A ₂ < 769 °C		
γ	Austenite	A ₃ ; 911 °C - 1392 °C	Solid solution	
Fe ₃ C	Cementite		Stoichiometric, Intermediate Phase	
Perlite (P)	α-phase + Fe ₃ C	A ₂ ; 723 °C	Eutectoid	Point S
Ledeburite I (L ₁)	γ-phase + Fe ₃ C	A ₂ > 723 °C	Eutectic	
Ledeburite II (L ₂)	P + Fe ₃ C	A ₂ < 723 °C	Eutectic	
α'	Martensite	< 430 °C	Solid solution	

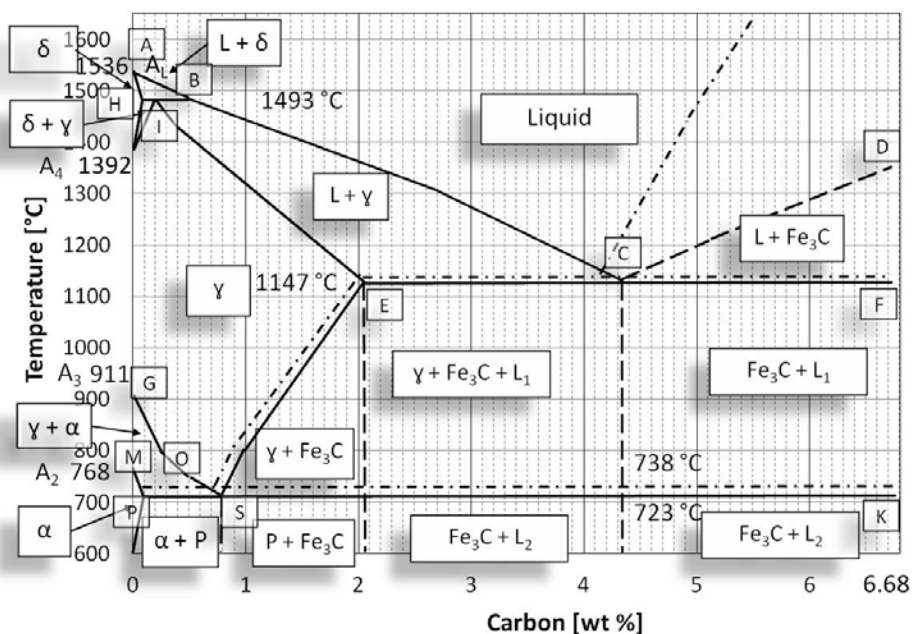


Fig. 2. Binary phase diagram of Fe-C and Fe-Fe₃C system; with phase areas [8].

1.3.1. Partial systems in the Fe- Fe₃C diagram

The metastable Fe-Fe₃C system consists of three partial systems. These are summarized in Fig. 3.

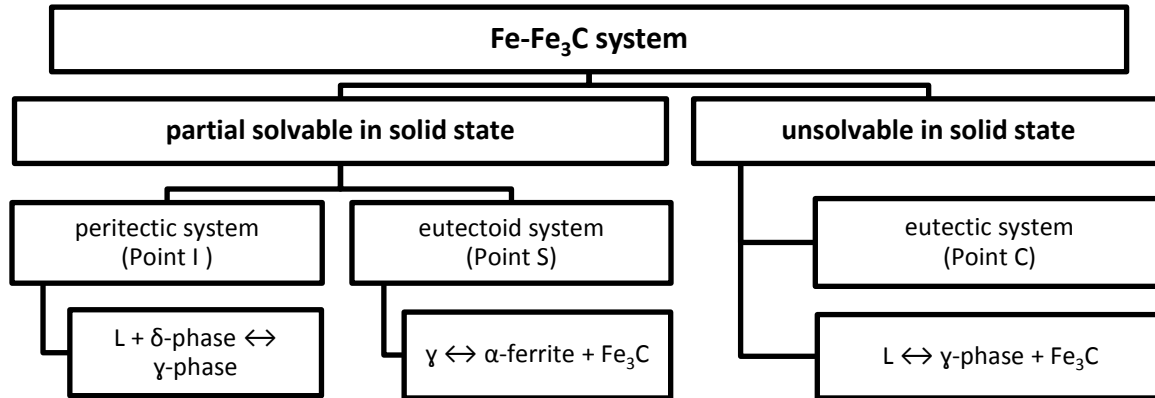


Fig. 3. Partial systems in metastable Fe-Fe₃C system [8].

The partial peritectic-system is characterized by the transformation of the mixture of liquid and (solid) δ -ferrite phase into a pure γ -austenite phase below the peritectic temperature of 1493 °C, when the carbon content is greater than 0.1 mass % (same as wt %).

Of a greater technical relevance is the partial eutectoid system (Line G-O-S-E in Fig. 2), where a transformation of the austenite into α -ferrite and Fe₃C occurs. A complete decomposition of austenite into α -ferrite and Fe₃C-cementite only occurs in alloys with carbon content (C) more than 0.8 mass %, where the α -ferrite is one phase in the perlite (P) phase. When the carbon content equals 0.8 mass %, and the temperature is below A₃ (723 °C), the material transforms into a completely perlite phase (Point S). Steel alloys with 0.02 mass % \leq C < 0.8 mass % (Line G-O-S) are called hypo-eutectoid steels. When the carbon content is less than 0.8 mass %, the material is a mixture of α -ferrite and perlite phases. A complete α -ferrite phase exists when the carbon content is less than 0.02 mass %. In contrast, when the carbon content is greater than 0.8 mass % (up to 2.06 mass %), the material is considered to be a hyper-eutectoid steel (Line S-E) and is a mixture of perlite and Fe₃C phases.

In addition to carbon, other elements also affect the Fe-Fe₃C system phases. These can be observed by a change of the transformation temperatures, a change of the solvability of carbon or other elements, a change of diffusion processes, and a formation of new solid phases, e.g., intermetallic and or intermediate. For steels, these mostly fall into two groups that affect the formation of the α -ferrite and austenite. The first group consists of elements that expand the γ -area in the Fe-Fe₃C-system (phase diagram). These are referred to as austenite stabilizing elements. Other than carbon, the most relevant austenite stabilizing elements are nickel (Ni), manganese (Ma), cobalt (Co), rhodium (Rh), copper (Cu), and nitrogen (N / N₂). In contrast, the second group consists of ferrite stabilizing elements, which reduce the γ - area in the phase diagram by increasing the austenite transformation temperature (A₄). These ferrite-stabilizing elements include aluminum (Al), chromium (Cr), molybdenum (Mo), silicon (Si), and titanium (Ti) [2,8].

1.4. Phase transformations during cooling

As described in previous sections, the existence of certain phases in steel, such as austenite, perlite, α -ferrite, δ -ferrite, and Fe₃C, depend on the chemical composition and the amounts of certain elements at different temperatures. The formation of these phases in the metastable Fe-Fe₃C system is based on the assumption of very slow cooling in order to obtain equilibrium. In

manufacturing processes such as casting, welding, and additive manufacturing, the cooling rates are significantly higher than the equilibrium assumption and can impact the phase transformations in a Fe-Fe₃C- system. As a result, other phases in the material structure can occur, which cannot be described by the binary Fe-Fe₃C- diagram. For example, an increase in cooling rate causes a finer lamellar structure of the perlite phase. A further increase in cooling rate causes the transus temperatures of the γ - α - transformation (A₃) and that of the perlite formation to be combined resulting in no perlite formation. Table 4 summarizes the effect of different cooling rates on the resulting microstructure.

Table 4. Correlation between cooling rates and obtained microstructure [9].

Cooling rate [°C / s]	Transition point indicator	Transus temperature [°C]	Micro structure	C- content [mass %]	Comment
< 1	A ₁	723	Perlite	0.8	Equilibrium
	A ₃		+ Ferrite	(< 0.8)	
	A _{cm}		+ secondly Fe ₃ C	(0.8 to 2.06)	
1 to 200	A	690 to 600	Fine Perlite (Sorbite)	0.24 to 2.06	Perlitic formation
200 to 250 (500)	A	600 to 500 (460)	Very fine Perlite (Troosite)	0.24 to 2.06	Perlitic formation
250 to 600	M _S	430 to 98	Martensite	> 0.24 (0.5)	Lattice shearing
> 600	M _F	(300) to < 0	Retained austenite	> 0.24 (0.5)	Lattice shearing

The failure of the perlite formation is due to the suppression of the solid-state diffusion resulting from the high cooling rate. Other phases, which are independent of the diffusion processes of the contained elements, may be formed. However, these phases cannot be described in the Fe-Fe₃C-phase diagram.

1.4.1. Martensite formation

After reaching the critical cooling rate that is high enough to suppress the solid-state diffusion of dissolved carbon atoms during the transformation of FCC γ - phase (austenite) into a BCC lattice structure, the lattice structure is deformed and the nucleation of a martensite grain grows rapidly through the material until it approaches another grain boundary. As shown in Figure 4, when the cooling rate is fast enough, the dissolved carbon in the austenite cannot diffuse out of the FCC lattice structure, leading to a tetragonal lattice distortion [5,7, 9, and 10], i.e., martensite is a tetragonal distortion of α - ferrite. Furthermore, an incomplete martensite transformation can be continued at a later time, even when the material has already reached room temperature by an additional annealing or a sub-zero temperature treatment. The critical temperature where the martensite nucleation begins is called “martensite starting temperature” (M_S) and the temperature where the entire material microstructure is martensite is known as “martensite finish temperature” (M_F).

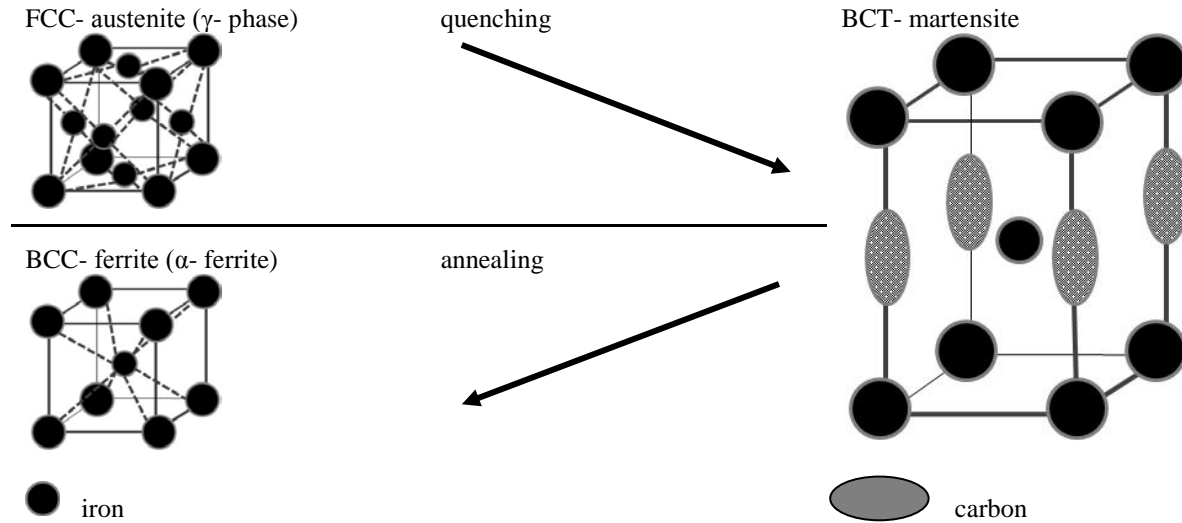


Fig. 4. Schematic martensite formation with forced solid solved carbon in BCT lattice structure [7].

Depending on temperature and chemical composition of steels, martensite can be formed in two different morphologies. Hypo eutectoid ($0.02 \text{ mass \%} \leq C < 0.8 \text{ mass \%}$) steel alloys show predominant lath martensite, which has better plastic formability than plate martensite. Plate (twinned) martensite is predominant in hyper eutectoid ($0.8 \text{ mass \%} < C \leq 2.06 \text{ mass \%}$) steel alloys. Even though M_F may be reached, depending on the amount of carbon, some amount of austenite still exists. The existence of this retained austenite can be explained by the high inner stress caused by the lattice structure distortion during the martensite formation, preventing further nucleation of the martensite grains [5, 9,10]. Most alloying elements, which are soluble in austenite, cause a decrease in M_S and M_F . Based on the chemical composition, the approximate M_S of steel can be computed by Eq. (1) [11]. We note that this equation does not include the effect of cooling rate and the inhomogeneous distribution of the elements.

$$M_S [^{\circ}\text{C}] = 539 - 423 \cdot C\% - 7.5 \cdot Si\% - 30.4 \cdot Mn\% - 12.1 \cdot Cr\% - 17.7 \cdot Ni\% - 7.5 \cdot Mo\% - 10 \cdot Co\% \quad (1)$$

The computed M_S for S17-4 and S15-5 using the element content in Table 1 are $167.5 \text{ }^{\circ}\text{C}$ and $184.3 \text{ }^{\circ}\text{C}$, respectively. Reference [12] refer to a M_S of $132 \text{ }^{\circ}\text{C}$ and a M_F of $32 \text{ }^{\circ}\text{C}$ for welds of S17-4 steel plates. However, they did not mention how the M_S and M_F temperatures were obtained.

Table 5. Chemical composition of the virgin stainless steels S17-4 and S15-5 powders as reported by the powder supplier [13, 14].

Element content, [mass %]	Chemical composition of virgin stainless steel powder, S17-4	Chemical composition of virgin stainless steel powder, S15-5
Carbon; C	≤ 0.07	≤ 0.07
Manganese; Mn	≤ 1.00	≤ 1.00
Phosphorus; P	-	-
Sulfur; S	-	-
Silicon; Si	≤ 1.00	≤ 1.00
Nickel; Ni	3.00 - 5.00	3.50 - 5.50
Chromium, Cr	15.00 - 17.50	14.00 - 15.50
Molybdenum; Mo	≤ 0.5	≤ 0.3
Copper; Cu	3.00 - 5.00	2.50 - 4.50
Nitrogen; N	-	-
Tantalum Ta + Niobium Nb	0.15 - 0.45	0.15 - 0.45
Iron; Fe	Balance (69.5)	Balance (71.7)

A further transformation of the retained austenite into martensite can be realized by an additional heat treatment, which relieves the high inner stress to continue growing the martensite grain. Reference [6] summarized the different heat treatments for different steel alloys to achieve specific material properties. A post annealing heat treatment at temperatures approximately between 200 °C and 300 °C causes an expansion of the material volume. This phenomenon can be explained by a re-initiation of the transformation of the retained austenite into martensite [6]. Holding the steel at these temperatures for a longer period of time increases the strength and the toughness of the steel. This is known as tempering, which is characterized by a transformation of a tetragonal martensite into a cubic martensite and a further transformation to a $Fe_{\approx 2}C$ phase (ϵ -carbide, hexagonal). Further heating leads to a transformation of ϵ -carbide into the intermediate phase Fe_3C and might continue to decompose retained austenite into martensite, which can be observed by a dilatation of the material [6]. In some cases, subzero heat treatment is highly recommended for highly alloyed stainless steels to transform the retained austenite into martensite [15].

1.4.2. Metallurgical characteristics of corrosion-resistant steel alloys manufactured by welding

Depending on their chemical composition, corrosion resistant Cr-Ni steel alloys solidify in either primary ferritic or primary austenitic phases. The solidification of two different Cr-Ni steel alloys, with iron content of approximately 72 mass % and varying relative amounts of equivalent chromium and nickel contents (also called “chromium-equivalent” and “nickel-equivalent”), is schematically shown in a three phase-reaction diagram [16]. As shown in Fig. 5, the ratio of the chromium- and nickel- equivalents (Cr_{Equ} / Ni_{Equ}) is a determining factor for primary ferritic and austenitic solidification. The amount of δ -ferrite during the solidification decreases with a decreasing Cr_{Equ} / Ni_{Equ} ratio.

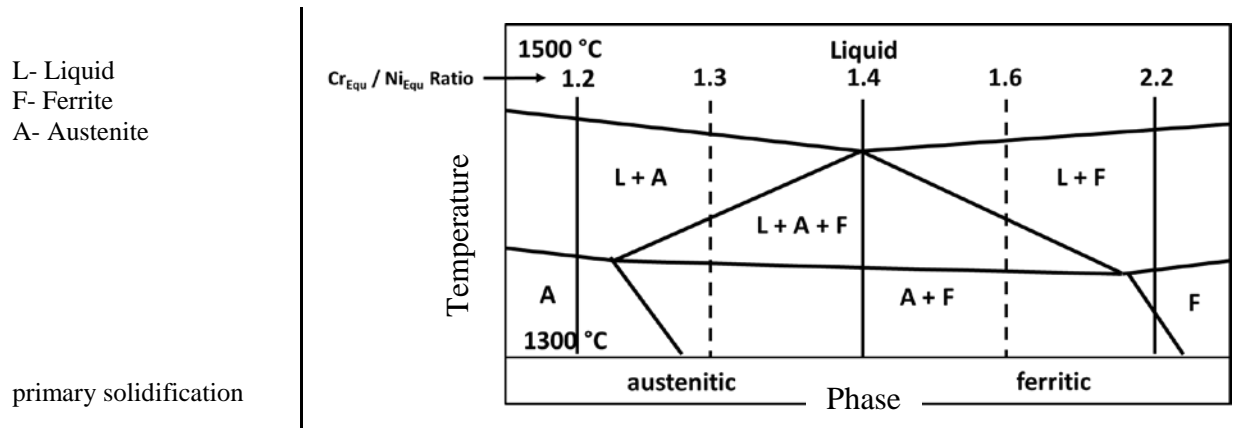


Fig. 5. Illustration of three phase solidification diagram [16].

The amount of and the ratio between certain elements lead either to a dominant formation of FCC γ -austenite, BCC δ -ferrite, BCC α -ferrite, or to formation of coherent and incoherent precipitants during the solidification of an austenitic, martensitic, ferritic, dual phase (DP) of austenite and ferrite, and tri phase (TP) stainless steels. The ferrite and austenite stabilizing elements are considered in the Cr- and Ni- equivalents and used to predict the solidified microstructure of welds. Depending on their chemical composition and cooling rate, primary ferritic (δ -ferrite) Cr-Ni steels can be further differentiated in two sub-groups: in one group the δ -ferrite further transforms into γ -austenite during cooling and in the other group the δ -ferrite exists even at low temperatures. The reason for the existence of δ -ferrite at room temperature is either the chemical composition or the high cooling rate, preventing a transformation into austenite. The δ - to γ - phase transformation only occurs at high temperatures (A_4) between 1392 °C and 1493 °C (see Fig. 1) and the γ -phase starts at the grain boundary of the δ -phase and grows into the grain center. If the ferrite is formed as intra dendrite or cells, then the alloy will solidify as primary δ -ferrite, which will partially transform at a later time into γ -phase.

In both cases, the austenite, which still remains at room temperature, is metastable. When it is exposed to higher temperature, it begins to decompose into other phases, like the BCT martensite, α -ferrite, or forms with other elements or incoherent precipitants like carbides.

The transition from stable δ -ferrite to metastable γ -austenite was examined by several researchers in the welding field. Reference [17] presented that the primary phase and microstructural morphologies were affected by the composition and solidification rate of the primary δ -phase and γ -phase. References [18 and 19] explained the δ - to γ - transformation through the kinetic process of the dendrite growth. Reference [20] observed that the formation of metastable γ -austenite occurred in substantially undercooled melt pools. References [21 and 22] claimed that the formation of primary γ in Fe-Cr-Ni alloys was controlled at the nucleation stage due to the ease of the δ -phase nucleation from the undercooled melt pools. Reference [23] observed the eutectoid structure of fine dispersed primary δ -ferrite and γ -austenite in Fe-Cr-Ni- alloys during laser treatment with high cooling rates. Reference [24] developed a general dendrite growth model for directional solidification including rapid solidification conditions. The developed diagrams indicated the microstructures (plane front, dendrite/cell, eutectoid, and bands) which resulted from the growth competition between the several microstructure morphologies of both stable and metastable phases.

Laminal spacing measurements of the obtained eutectic structure on different laser treated Fe-Cr-Ni alloy were made by [25]. They examined the relationship between average laminal spacing to various local solidification velocities (V_s), which were evaluated at the surface of the remelted zone. V_s was determined by scanning speed of the laser beam and the angle between the scanning direction and the direction of the interfacial motion evaluated through the form of the liquid pool at the surface of the specimen. This procedure is acceptable if the dendrite growth axis lies in the surface [25].

Figure 6 **Error! Reference source not found.** shows the microstructures of the Cr-Ni stainless steel alloy, which was treated with various laser scan velocities leading to various solidification velocities (V_s) of the growing dendrite through the melt. Dark and bright areas represent δ -ferrite and γ -austenite. Lower laser velocities lead to lower solidification velocity which could be detected with a wider spacing between the dendrites (λ), for example: $\lambda = 63 \mu\text{m}$ at $V_s = 1.7 \mu\text{m/s}$ (b) and $\lambda = 26 \mu\text{m}$ at $V_s = 1000.0 \mu\text{m/s}$ (d). The laminal stable δ -cells were observed at medium growth rate of $V_s = 400 \mu\text{m/s}$ as shown in Fig. 6c. Metastable γ -dendrites were observed in the material what was treated with high velocity of the laser beam (see Fig. 6d).

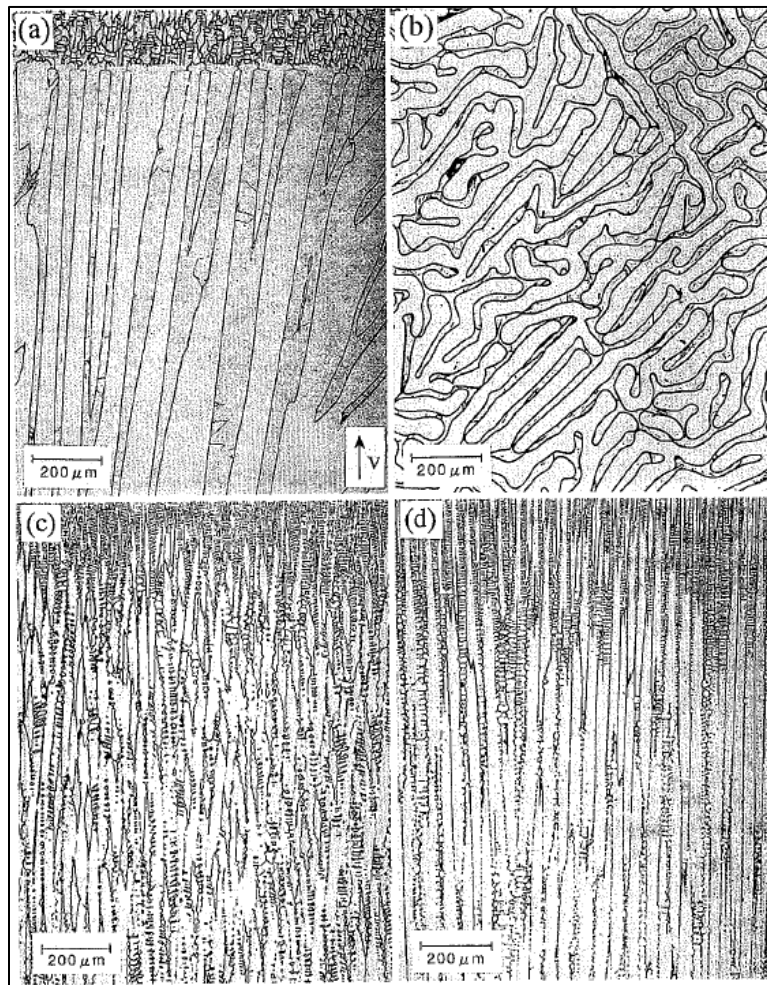


Fig. 6. Microstructure obtained with different laser treatment parameters, a) longitudinal section of eutectic structure at $V_s = 1.7 \mu\text{m/s}$, b) cross section of a, c) stable δ - cells at $V_s = 400 \mu\text{m/s}$, and d) metastable γ - dendrites at $V_s = 1000 \mu\text{m/s}$ [25].

1.4.3. Corrosion resistant Cr-Ni stainless steel alloys used in additive manufacturing applications

Prediction of the solidified material structure and associated material properties after a laser-based fabrication process is important. Steel alloys with high amounts of Cr and Ni are widely used for the fabrication of functional components by additive manufacturing technology. Welding of Cr-Ni steel alloys by tungsten inert gas (TIG) or by a laser source are similar to the PBF process in the sense of thermal treating the material. Cr-Ni steel alloys show occasionally a risk of hot cracking along the boundary between the welding seam and the heat affecting zone (HAZ). This phenomenon is well known and caused by micro segregation during the solidification of metastable FCC austenite (γ -phase).

Two martensitic precipitation-age-hardening Cr-Ni stainless steel alloys (S17-4 and S15-5) were used in this study to investigate the effectiveness of methods for the prediction of microstructure evolution during the powder bed fusion process. S17-4 and S15-5 conform to ASTM A564 [26]. S17-4 in solution-annealed condition is characterized with good machinability, which may be age-hardened to the specified mechanical properties. The main reason for the high corrosion resistance is the high amount of chromium between 15.00 mass % to 17.00 mass %, which forms an unreactive passive layer on the material surface. The predominant BCT- martensite microstructure in S17-4, after a solution heat treatment and quenching, can be post hardening heat treated, which causes the formation of non-coherent FCC copper- (Cu-) rich precipitants [27]. The recommended maximum operating temperature for solution annealed and quenched S17-4PH is around 315 °C, because of the high risk of stress corrosion cracking due to the retained austenite. Hence, austenite should only exist in a stable form or the post-heat treatment defined by cooling and aging should be adopted in order to avoid the existence of retained metastable austenite in the final S17-4 material. The same is also true for temperatures below -18 °C. Depending on the post annealing after the quenching, the transformation of the retained austenite into Cu- depleted martensite, stable austenite, and some amount of ferrite and primary austenite occurs at this temperature. In general, during the cooling from temperatures above 600 °C, the transformation to martensite begins below 200 °C (M_s) and may not be fully completed at room temperature. Therefore, before the post-aging heat treatment begins, a sub-zero-temperature treatment at -50°C or an aging at room temperature for hours are highly recommended [7,15].

2. Prediction of microstructure transformation

Microstructure of Cr-Ni stainless steel alloys resulting from the LPBF process significantly affects material performance. For example, martensite increases the risk of inter grain material cracks caused by the hardening effect, while greater amounts of metastable retained austenite increases the risk of hot cracking. The formation of sigma (σ) phases can lower the ductility in zones where both phases of austenite and δ -ferrite coexist. Therefore, the ability to predict the contents of martensite and austenite phases of Cr-Ni stainless steel alloys manufactured using LPBF processes will be a major advancement in the AM field. Manufacturers will be equipped to design the process through careful selection of the metal powder, build process conditions, and / or adapting the post-process heat treatment procedure to achieve parts that meet their full performance potential.

2.1. Isothermal and continuous cooling microstructure prediction

An isothermal Time-Temperature-Transformation (TTT) diagram allows the microstructure transformation to be predicted as the material cools from above the austenite transus temperature

(A₃) to the final temperature and then held constant for a long period of time (e.g., for multiple hours). As an example, Fig. 7 shows the TTT diagram of a stainless steel alloy (X36Cr13).

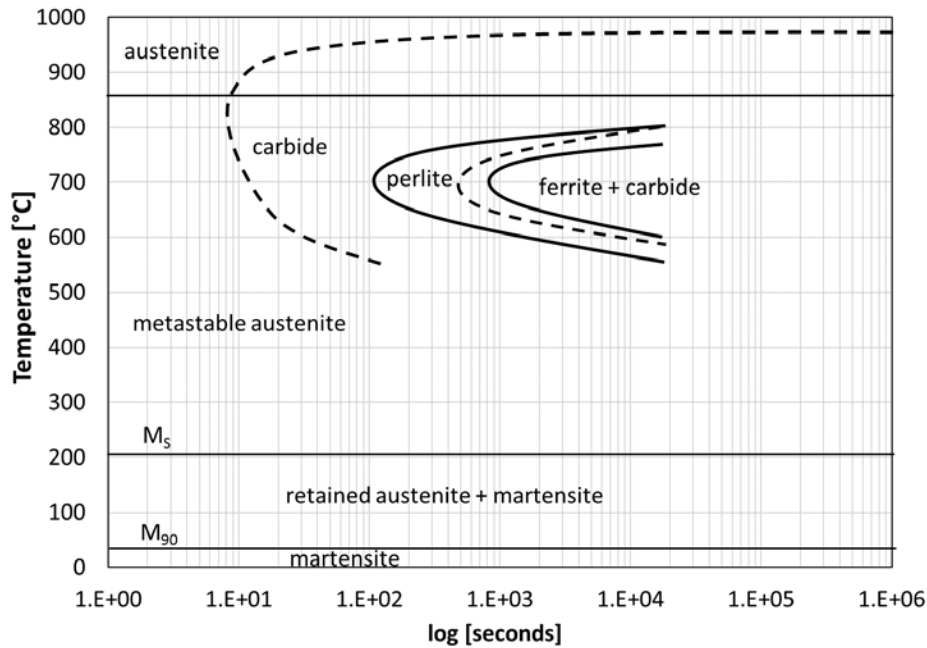


Fig. 7. Isothermal TTT Diagram of a martensitic stainless steel type X39Cr13 (similar to AISI 420C) [28].

In contrast to an isothermal TTT diagram, the development of a continuous cooling transformation (CCT) diagram requires the steel specimens to continuously cool down with different cooling rates from above the austenite transus temperature. Furthermore, CCT diagrams allow assessing phase transformations and their related effect on the mechanical properties. CCT diagrams also allow the critical cooling rates to be determined (see Fig. 8). For instance, the cooling rate where martensite begins to occur in the microstructure is called the lower critical cooling rate. The upper critical cooling rate defines the rate, where only martensite exists after reaching room temperature.

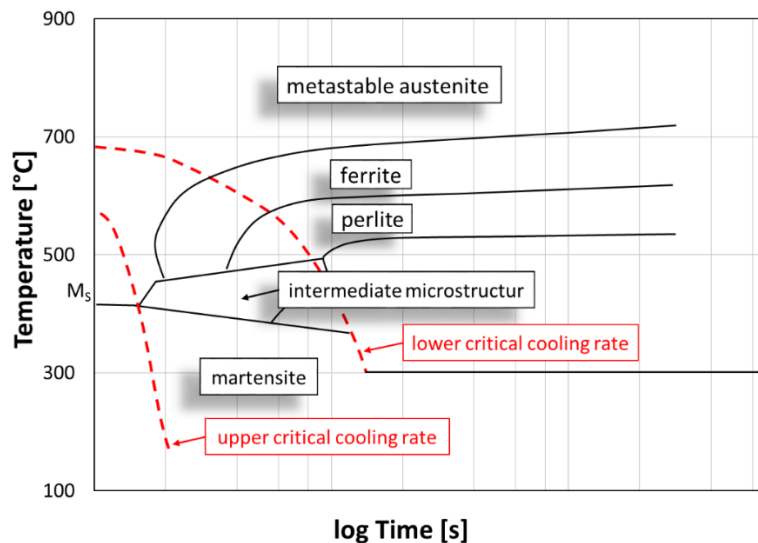


Fig. 8. Continuous Cooling Transformation (CCT) diagram, [10].

2.2. The prediction of microstructure in welding applications

In welding applications, which experience rapid cooling during the process, two diagrams are primarily used to predict the resulting material microstructure. The Schöffler diagram is the most accepted microstructure prediction diagram and it is commonly used for estimating the δ -ferrite content of stainless steel weld metals [2]. The Schöffler diagram (Fig. 9) shows phase fields and iso-ferrite lines of microstructure of a weld depending on its chemical composition. It is not an exact phase diagram but an approximation, which helps to predict the microstructure at room temperature after cooling from high temperatures [29].

The Schöffler diagram helps to predict the existence of ferritic, martensitic, and austenitic phases in corrosion resistant steels with carbon content up to 0.25 mass % as a function of Cr_{Equ} and Ni_{Equ} [30]. As shown by Eq. (2), Cr_{Equ} represents the weighted sum of the elements Chromium (Cr), Silicon (Si), Molybdenum (Mo), Titanium (Ti), and Niobium (Nb), which promote the formation of δ -ferrite. Ni_{Equ} represents the weighted sum of the elements Nickel (Ni), Manganese (Mn), and Carbon (C), which promote the γ -austenite formation (see Eq. (3)) [2].

$$Cr_{Equ} = Cr\% + 1.5 \cdot Si\% + Mo\% + 2.0 \cdot Ti\% + 0.5 \cdot Nb\% \quad (2)$$

$$Ni_{Equ} = Ni\% + 0.5 \cdot Mn\% + 30 \cdot C\% \quad (3)$$

Table 6 contains the computed Cr_{Equ} and Ni_{Equ} values and the the Cr_{Equ} / Ni_{Equ} ratio for both S17-4 and S15-5 according to Eqs. (2) and (3) and the chemical content listed in Table 5. The computed Cr_{Equ} / Ni_{Equ} ratios of 2.6 for S17-4 and 2.2 for S15-5 indicate that both alloys will presumably be primarily ferritic (δ -ferrite) when they solidify, as previously shown in Fig. 5.

Table 6. Computed Chromium-Equivalent (Cr_{Equ}) and Nickel-Equivalent (Ni_{Equ}) values for S17-4 and S15-5.

Chromium- (Cr_{Equ}) and Nickel-Equivalent (Ni_{Equ})	stainless steel; S17-4	stainless steel; S15-5
Cr_{Equ}	19.7	17.5
Ni_{Equ}	7.6	8.1
Cr_{Equ} / Ni_{Equ}	2.6	2.2

Figure 9 shows areas on the Schöffler Diagram, indicating different phases that occur based on the chemical content of the steel (represented by Cr_{Equ} and Ni_{Equ}). Alloys that are commonly referred to as martensitic or austenitic typically lie within the regions outlined by the two bold boxes. The diagram illustrates that each alloy can contain some fraction of ferrite, while the martensitic alloys can also contain some portion of austenite. Alloys located in the transition zone where all three phases can coexist are referred to as “soft martensitic steels”.

The specific alloys studied in the current work are indicated on the diagram based on the calculated values of Cr_{Equ} and Ni_{Equ} presented in Table 6. S17-4 is represented by the black circle and S15-5 is represented by the black square (see Fig. 9). These alloys clearly lie in the transition region in which martensite, austenite, and ferrite can co-exist and can be considered as soft martensitic steels. Using the diagram in Fig. 9, one can predict that S17-4 will contain an amount of δ -ferrite between 20 % and 40 % and S15-5 will have a lower fraction of δ -ferrite, between 5 % and 10 %. As described previously using the CCT diagram, this microstructure is caused by the rapid cooling, between the lower and upper critical cooling rates and the specifically high content of alloying elements.

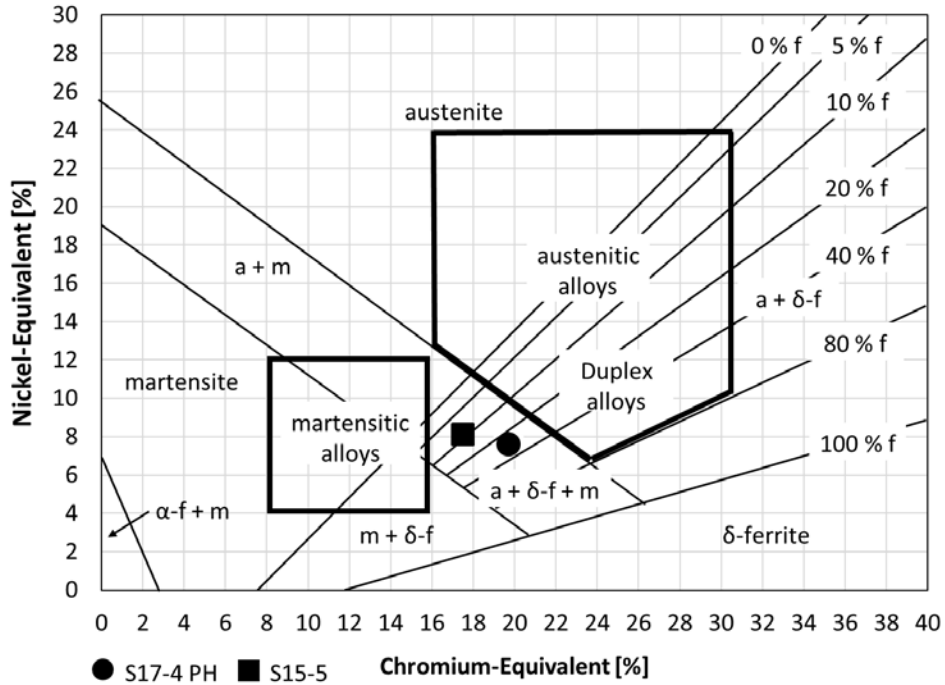


Fig. 9. Possible microstructure of S17-4 and S15-5 according to the Schäffler Diagram [2], percentage of ferrite (% f)

2.3. The inclusion of nitrogen in the microstructure prediction

Originally the Ni_{Equ} value (see Eq. (3)) used in the Schäffler Diagram did not account for an increase in nitrogen during the manufacturing process. In the 1970's DeLong amended the diagram and the associated equation for $Ni_{Equ-mod}$ (Eq. (4)) to allow for the possibility of adding controlled percentages of nitrogen (N%) to the alloy during the manufacturing processes [3,31].

$$Ni_{Equ-mod} = Ni\% + 0.5 \cdot Mn\% + 30 \cdot C\% + 30 \cdot N\% \quad (4)$$

The S17-4 and S15-5 metal powders considered in this study are produced using gas atomization in a nitrogen atmosphere and the PBF process is carried out in a nitrogen flooded chamber. Therefore, it is reasonable to assume that the produced alloy will have an increased nitrogen content.

Furthermore, dual phase ferritic-austenitic steel alloys often contain copper (Cu) in the amount of more than 2 mass %. Several studies [32 - 35] have shown the effect of varying Cu contents on the material structure of these alloys. To accommodate the influence of Cu, the $Ni_{Equ-modCu}$ was further modified as shown in Eq. (5) [36, 37].

$$Ni_{Equ-modCu} = Ni\% + 0.5 \cdot Mn\% + 30 \cdot C\% + 30 \cdot N\% + 0.25 \cdot Cu\% \quad (5)$$

The calculated Cr_{Equ} , $Ni_{Equ-mod}$, $Ni_{Equ-modCu}$, values for S17-4 and S15-5 are presented in Table 7 and indicated on the DeLong diagrams presented in Fig. 10 and Fig. 11, respectively. In order to demonstrate the possible impact of nitrogen on the resulting phases, these diagrams are created assuming a range of N_2 content up to 0.15 mass % for both S17-4 and S15-5, respectively. The maximum assumed value of 0.15 mass % nitrogen content is consistent with the results from Ref. [38]. They measured a nitrogen content of 0.17 mass % in a S17-4, which is additively manufactured in a nitrogen environment using nitrogen atomized S17-4 powder [38].

Table 7. Calculated modified nickel-equivalents values; $Ni_{Equ-mod}$ and $Ni_{Equ-modCu}$ for S17-4 and S15-5 depending on the content of nitrogen and copper.

Content of N ₂ [mass %]	stainless steel; S17-4 5 mass % Cu			stainless steel; S15-5 4.5 mass % Cu		
	$Ni_{Equ-mod}$	$Ni_{Equ-modCu}$	$Cr_{Equ} / Ni_{Equ-modCu}$	$Ni_{Equ-mod}$	$Ni_{Equ-modCu}$	$Cr_{Equ} / Ni_{Equ-modCu}$
0.00	7.6	8.9	2.2	8.1	9.2	1.9
0.05	9.1	10.4	1.9	9.6	10.7	1.6
0.15	12.1	13.4	1.5	12.6	13.7	1.3

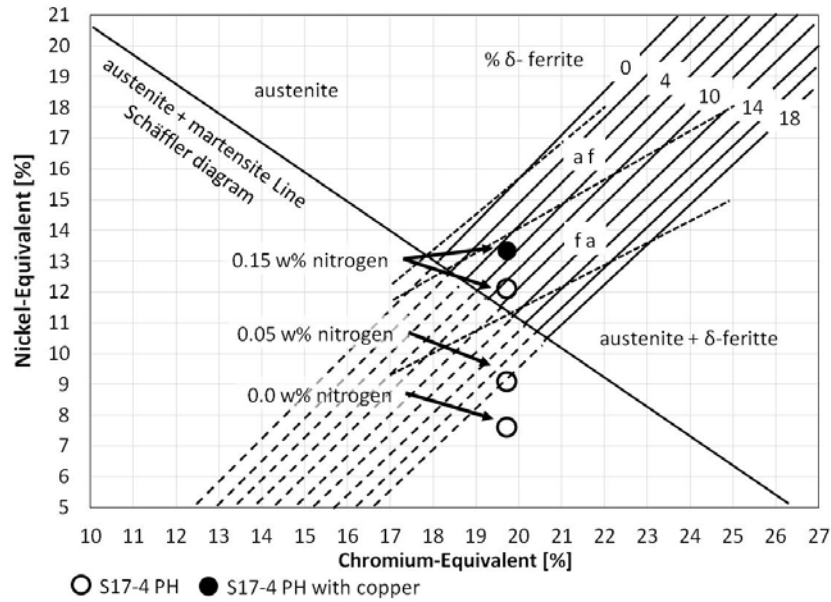


Fig. 10. Possible microstructure of S17-4 according to the Delong Diagram and equations for Cr_{Equ} , $Ni_{Equ-mod}$, and $Ni_{Equ-modCu}$, percentage of δ - ferrite (% δ -f).

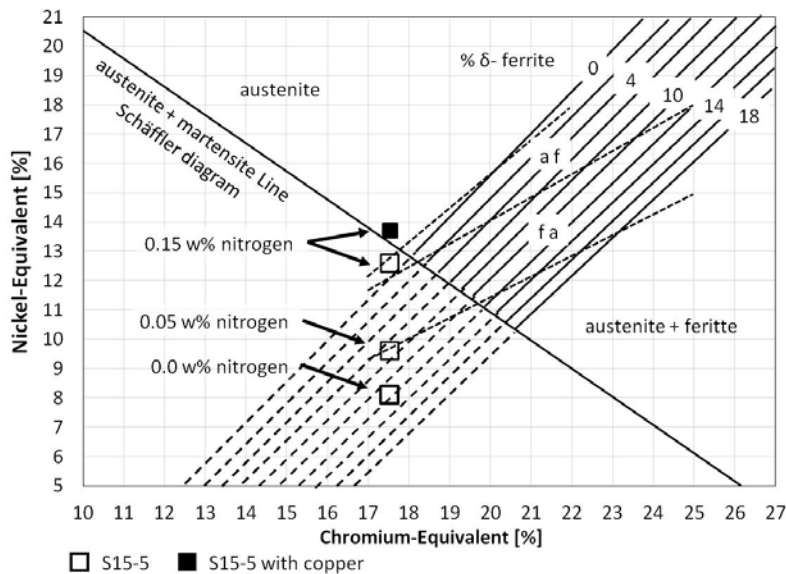


Fig. 11. Possible microstructure of S15-5 according to the Delong Diagram and equations for Cr_{Equ} , $Ni_{Equ-mod}$, and $Ni_{Equ-modCu}$, percentage of δ - ferrite (% δ -f).

Figure 10 shows that increasing the percentage of nitrogen in S17-4 decreases the percentage of δ -ferrite from more than 20 % (as previously shown in the Schäffer diagram in Fig. 9), down to less than 8 % with an N_2 content of 0.15 mass %. In the case of S15-5, the same increase in nitrogen removes all ferrite and produces a phase that is nearly all austenite, especially when copper is included, as shown in Fig. 11. Unfortunately, greater amounts of metastable γ -phases (γ -austenite) increases the tendency of the material to experience hot cracking. In addition, the presence of nitrogen in the case of soft martensitic stainless steel alloys, such as S17-4 and S15-5, also decreases the amount of martensite, which decreases hardness and toughness. The Cu content for both steels, as shown in Table 5, significantly affects the prediction and should therefore be considered when predicting the amount of δ -ferrite.

These results presented in Fig. 10 and Fig. 11 indicate that any amount of nitrogen stabilizes the formation of the γ -austenite and causes a decrease of δ -ferrite. Furthermore, these predictions for the material microstructure of LPBF manufactured S17-4 are consistent with observations from Ref. [38], who reported a predominant γ -phase (99.3 %) in the S17-4, when the nitrogen gas atomized S17-4 metal powder was used in the LPBF build in a N_2 environment, resulting in nitrogen content in the manufactured material equaling 0.17 mass %. In contrast, argon (Ar) atomized S17-4 powder led to a predominant martensitic S17-4, (87 % martensite) [38].

Therefore, the process atmospheres during the powder production and during the AM build have a significant impact on the powder and additively manufactured material microstructure. Reference [27] investigated the effect of different process gas atmospheres either in the powder production and later during the laser based PBF process on the microstructure and hardness of S17-4. Results of their hardness measurements indicated a predominant γ -phase even after the post heat treatment at a temperature of 482 °C for one hour with a hardness of about HRC 21, because the hardness values were significantly lower than of the Ar gas atomized and in an Ar build atmosphere fabricated S17-4 (\approx HRC 30). Reference [27] has not quantified the different amounts of δ -ferrite, austenite, α -ferrite, and or martensite, however the work shows effects of the powder and its production history on the microstructure and mechanical properties of LPBF manufactured material.

2.4. Stability of retained austenite in the microstructure

The amount of retained γ -austenite in Cr-Ni stainless steel can be either detrimental or beneficial to the part's performance, depending on its intended application. Therefore, the manufacturing process and subsequent heat treatment need to be planned accordingly. If the amount of γ -austenite stabilizing elements and/or the cooling rate are too high, it is possible that the austenite will not completely decompose into martensite and will remain after the material reaches room temperature. This retained austenite is metastable and will transform into martensite and intermediate carbides like Fe_3C , if subjected to cold-work. "Martensitic stress induced transformation" (*MIST*) [39], which can occur at room temperature, will transform the metastable austenite into martensite, ultimately changing the material properties from the initial manufactured state. Exposure to extreme temperatures (e.g., below martensite finish temperature, M_F) can also transform the metastable austenite [6]. The M_F can occur at subzero temperatures. If any of these conditions are met while the part is in service, it may no longer perform as expected or even fail. Therefore, understanding and controlling the stability of the retained austenite in Cr-Ni stainless steel parts is of the utmost importance.

In equilibrium, Fe-C system with a carbon content of 0.07 mass %, the transformation from austenite to ferrite occurs at 770 °C (see Fig. 1). This temperature is known as the austenite transus temperature, A_3 . A_3 is the beginning temperature of transformation when the material diffuses in a solid state from austenite into ferrite. The transformation into ferrite is completed at 704 °C, which is defined as A_2 . Increasing alloying content decreases transus temperatures. After an adequately designed heat treatment of solution annealing followed by a quenching, most wrought Cr-Ni martensitic stainless steels have a very small amount of austenite, which is retained along the prior austenite grain boundaries. The driving force for suppression of the transformation of the retained austenite into martensite is the high strain developed at the high-angle boundaries during the quenching [40]. Hence, beside the amounts of γ -austenite stabilizing elements, especially Ni and Mn, the average grain size, i.e., the population of grain boundaries, affect the stabilization of the austenite, after cooling to room temperature. These factors, the chemical composition of the retained austenite, the size/morphology of the austenite grains, and the micro constitution, affect the stability of the retained austenite phase [41]. Reference [42] reported the effect of refinement of austenite grains for suppressing the martensite transformation. They found that the grain sizes less than 1 μm are very effective at increasing the stability, due to an increase in the required elastic strain energy to initiate the martensitic transformation. Reference [43] showed a decrease of M_s from 115 °C to 110 °C as the grain size changed from 1 000 μm to 50 μm . For grain sizes smaller than 10 μm , M_s reached room temperature of 20 °C. They examined this effect of a grain size refinement on an AISI 420 surface treated by a laser.

A useful indicator of the austenite to martensite transformation is the temperature (M_{d30}) at which an amount of 50 % austenite to be transformed into martensite through cold-deformation at 0.30 mm / mm true strain. M_{d30} is calculated using Eq. (6) [44]. This equation not only accounts for the austenitic and ferritic stabilizing elements, it also incorporates the grain size, which is represented by the grain size number (GS). The determination of the grain size number is described in the ASTM standard E 112 [45].

$$M_{d30}[\text{°C}] = 551 - 462 \cdot \text{C}\% - 9.2 \cdot \text{Si}\% - 8.1 \cdot \text{Mn}\% - 13.7 \cdot \text{Cr}\% - 29 \cdot \text{Ni}\% - 18.5 \cdot \text{Mo}\% - 29 \cdot \text{Cu}\% - 68 \cdot \text{Nb}\% - 462 \cdot \text{N}\% - 1.42 \cdot (GS - 8.0) \quad (6)$$

The M_{d30} temperatures of the two alloys considered in the current study are calculated using the chemical contents presented in Table 5 and grain sizes found in the literature for similar materials. Non-heat treated LPBF manufactured S17-4 has been shown by Ref. [46] to have an average grain size of 0.37 μm . Using a web-based calculation tool², the resulting GS number for that material is 19.5. This value is assumed to be the same for both the S17-4 and S15-5 alloys. For each alloy, the calculated M_{d30} temperatures at a variety of N_2 contents are presented in Table 8. These sub-zero M_{d30} temperatures suggest that, as recommended by the literature [15], cryogenic treatment can transform the remained metastable austenite into martensite.

Table 8. Computed M_{d30} for S17-4 and S15-5 depending on their N_2 content.

Content of N_2 [mass %]	M_{d30} [°C]	
	S17-4	S15-5
0.00	-84.57	-53.47
0.05	-107.67	-76.57
0.15	-153.87	-122.77

² <http://mathewpeet.org/science/materials/grain-size/>, date of use: June, 2016

The calculated values of M_{d30} for both steels allow the assessment of the stability of the retained γ -phases in LPBF manufactured Cr-Ni stainless steels; the greater differences from the room temperature indicate more stable retained austenite. As the nitrogen content increases, the M_{d30} temperature decreases, as shown in Table 8. This occurs because nitrogen stabilizes the primary austenite formation, as shown in Fig. 10 and Fig. 11. This means that a greater amount of metastable γ -austenite can be retained at room temperature after the manufacturing process is completed. S17-4 has a greater tendency to form a primary ferritic (fa-) microstructure (see Fig. 10) compared to S15-5, which forms more a primary austenitic (af-) microstructure (see Fig. 11, for the nitrogen content of 0.15 wt%). S17-4 has a lower M_{d30} , that results in a higher stability of the retained γ -phase.

Reference [47] observed that the retained γ -austenite level linearly increased as the M_S temperature decreased. Using Eq. (1), M_S for S17-4 and S15-5 are calculated as 167.5 °C and 184.3 °C, respectively. Apparently, lower temperatures are required to decompose the fewer amounts of the retained γ -phase that remain along the prior austenite grain boundaries and were not completely transformed into martensite.

The amount of retained austenite in LPBF manufactured Cr-Ni stainless steels can be controlled by post process heat treatments. Possible treatments include solution-annealing with a controlled cooling regime, annealing, or a cryogenic treatment, i.e., sub-zero treatment. It has been demonstrated that a sub-zero treatment on a finished tool steel almost completely decomposes the retained γ -austenite into martensite among intermediate Fe_3C -cementite [48]. Therefore, a cryogenic or subzero treatment on laser based PBF manufactured Cr-Ni steel alloys can be an alternative treatment to a solution annealing heat treatment to decompose the amount of retained austenite.

3. Experimental validation: S17-4 manufactured by LPBF

To demonstrate the effectiveness of the predictions for the LPBF generated microstructure by Schaffler and DeLong diagrams, results of several previous studies were used. In one recent study, nine cylindrical specimens, as shown in Fig. 12, were arranged three-by-three on a 25.4 mm thick steel (AISI 1045) build platform [49]. The specimens were fabricated from nitrogen atomized virgin stainless steel powder (S17-4) using the processing parameters shown in Table 9. The chemical composition of the powder is provided by the supplier and is shown in Table 5.

After the PBF build, the specimens were removed using wire electrical discharge machining (EDM). The top and bottom surfaces were machined to satisfy the required specimen tolerances for roughness and parallelism for the Rockwell hardness measurement (scale HRC), according to the ASTM E18 [50]. Hardness tests were then performed to investigate the mechanical properties of the LPBF built S17-4 alloy as a surrogate for the microstructure measurements.

In another recent study [51], six tensile specimens were fabricated using nitrogen atomized S17-4 powder and the tensile properties of LPBF manufactured S17-4 material (see Fig. 13) were studied. After the LPBF build, the plate was heat treated for residual stress relief, specimens were removed by EDM, and the removed specimens were machined to final dimensions. Tensile tests were then conducted. These results are analyzed here to compare them with the effects of estimated microstructure.

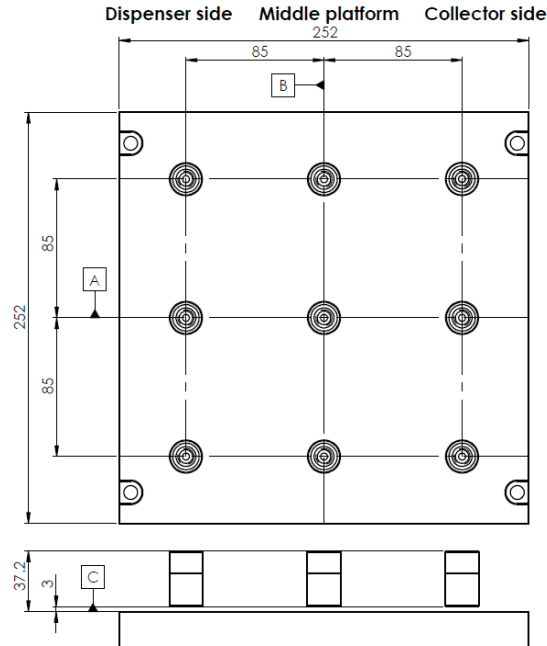


Fig. 12. Specimen arrangement on build platform, recoater direction parallel to Datum A moving from right to left. Dimensions are in mm.

Table 9. Nominal machine settings for this study.

Parameter	Skin	UpSkin	Post-Contour
Scan Pattern	Striped	Striped	x
Stripe Width	4 mm	4 mm	x
Laser Power (P_L) [W]	195	160	60
Scan Speed (v_L) [$1000 \text{ mm} \cdot \text{s}^{-1}$]	1000	500	700
Layer Thickness (t_L) [mm]	0.02	0.02	0.02
Assumed Laser beam diameter (d_L) [mm]	0.1	0.1	0.1
Raster Line Separation / Hatch (h_L) [mm]	0.1	0.1	X
Atmosphere	N_2	N_2	N_2
Volume Rate (VR) [$\text{mm}^3 \cdot \text{s}^{-1}$]	2.0	1.0	1.4
Energy Intensity (E_i) [$\text{J} \cdot \text{mm}^{-2}$]	1.95	3.2	0.86
Global Energy Density (E_G) [$\text{J} \cdot \text{mm}^{-3}$]	97.5	160.0	42.86

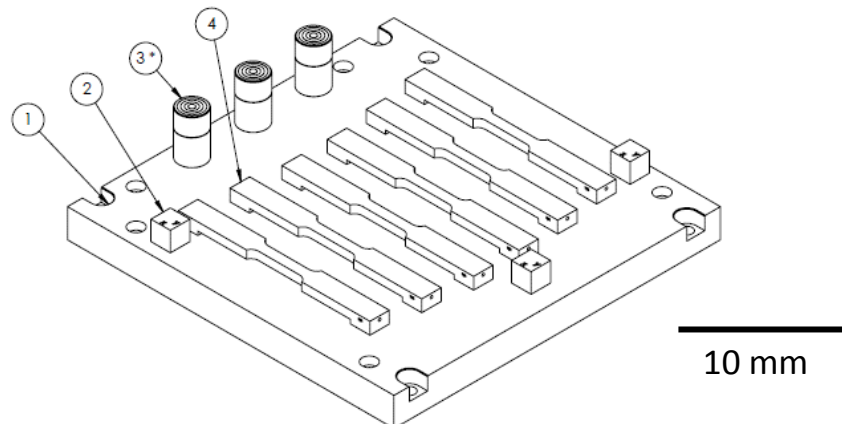


Fig. 13. Specimen arrangement for the second study showing build plate (1), witness cubes (2), powder collection capsules (3) and tensile specimens (4) [51].

The specimens were separately treated in cryogenic conditions. Based on the computed M_{d30} temperatures, as shown in Table 8, temperatures as low as $-154\text{ }^{\circ}\text{C}$, are required to transform 50 % of the retained metastable austenite in the additively manufactured S17-4 material. One option to realize a subzero heat treatment is submersion liquid N_2 , which has a boiling point at normal pressure of approximately $-196\text{ }^{\circ}\text{C}$ ($\approx 77\text{ K}$). Therefore, the specimens are submerged in liquid N_2 and removed after 1 minute. Another set of specimens was placed in a freezer for 4 hours at a temperature of $-80\text{ }^{\circ}\text{C}$. One of the specimens was not treated and tested in an “as-manufactured” condition to compare the effect of the cryogenic treatment.

4. Results and Discussion

Martensitic S17-4 [7, 52] has a predominantly FCC γ -phase in form as fine dispersed powder. Reference [51] found that the amount of the FCC γ -austenite in their LPBF parts was approximately 95 %. This large percentage of austenite was attributed to the nitrogen gas atomization to produce the S17-4 powder, which leads to a higher content of nitrogen in the material, as found by Ref. [38]. This assumption is consistent with the austenite stabilizing effect of N_2 in Cr-Ni stainless steel alloys, as previously calculated $\text{Ni}_{\text{Equ-mod}}$ (see Table 7) and shown on the Schöffler- and DeLong diagrams (see Fig. 9 and Fig. 10).

Although no significant martensitic transformation was observed, the increase in hardness was observed after post-process heat treatment, which is consistent with the literature [38, 53, and 54]. Reference [53] observed an approximately 12 % increase of the Vickers hardness after the S17-4 specimens were stress relief heat treated at a temperature of $650\text{ }^{\circ}\text{C}$. Furthermore, Ref. [53] investigated the effect of different heat treatments on the mechanical and metallurgical properties of laser based PBF manufactured S17-4. They found that a stress-relief heat treatment at a temperature of $650\text{ }^{\circ}\text{C}$ for only 1 hour did not affect the mechanical characteristics. They also found that the LPBF process ages the S17-4 as a result of the repetitive heating and cooling during the build process mimicking the heat treatment methods in a much smaller scale [53].

The amount of γ -austenite (stable and metastable) and intermetallic phases like the Fe_3C in S17-4 defines strength and toughness of this alloy. Aging heat treatment of quenched S17-4 causes formation of incoherent FCC phases (Cu and Nb) in the predominant BCT martensitic material structure, which contributes to an increase of strength and hardness. Usually a higher amount of BCT martensite and of its incoherent FCC phases results in a higher strength. Based on this relationship between the microstructure phases with the achieved mechanical material properties, one can assume which material phases in the stress relieved S17-4 exist after the laser based PBF.

The engineering stress-strain curves of the tested tensile specimens from Ref. [51] are shown in Fig. 14. The signal from the extensometer (Fig. 15A) shows an exhibited discontinuous yielding after passing the upper yield strength (UYS), i.e., a constant strength during continuous yielding of the material caused by initial movement of a dislocation front (Lüder Bänders) through the material. This is typical for soft, unalloyed steels with a low carbon content. This is also typical of the “softer” dominated austenite phase in the stress-relieved LPBF manufactured S17-4 material. Martensitic steels are usually characterized without an upper and lower yield strength (UYS and LYS) and without discontinuous yielding during the tensile test. The ultimate tensile strength (UTS) in Fig. 14B corresponds to maximum strain before the specimens failed.

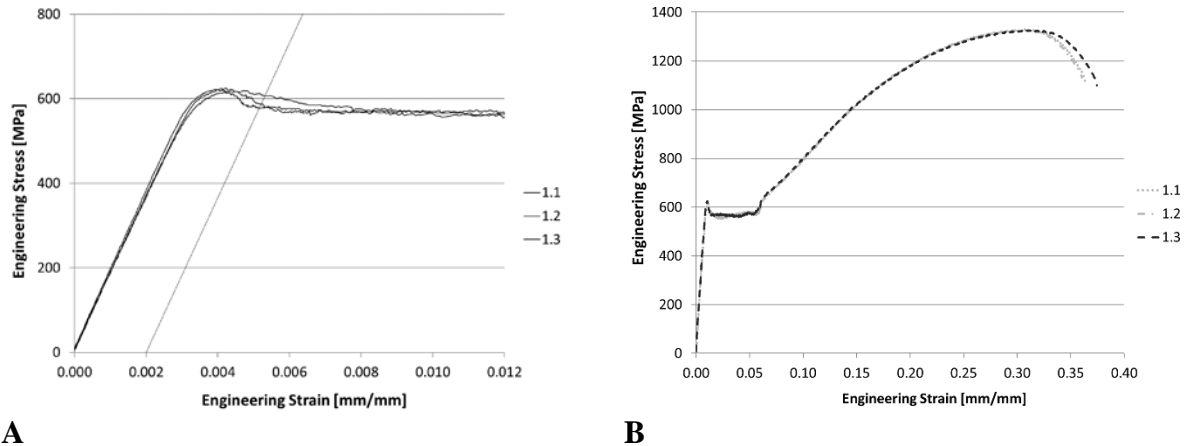


Fig. 14. Tensile stress strain curves of PBF manufactured S17-4 in stress-relief heat treated condition; extensometer signal (A) and maximum strain (B) [51].

Reasons for the high UTS above 1300 MPa and an elongation (A) of more than 20 % are the micro columnar, austenitic- martensitic- ferritic- material microstructure and the “martensitic stress induced transformation”, which occurs during the tensile test and leads to a very large elongation prior to failure. The transformation from FCC austenite into BCC martensite can occur due to cold working / plastic deformation as well as by rapid cooling from above A_3 [39]. Such transformation results in a change of the magnetism from paramagnetic to ferromagnetic.

Reference [38] investigated the effect of heating on LPBF manufactured S17-4 at temperatures of 650 °C and 788 °C to the conversion of the retained austenite. Their results of the high temperature X-ray diffraction (XRD) measurement showed a “little” conversion of the austenite for 650 °C heat treatment and substantial conversion for the 788 °C heat treatment. Results of the ferriteoscope measurements during the tensile tests showed that a transformation of the retained austenite into martensite initiated after passing the yield point and continued until failure [38]. A final amount of 50 % martensite was obtained after the plastic deformation ended. Those results prove the existence of decomposable retained austenite in LPBF produced S17-4, either in “as-manufactured” or 650 °C stress-relief heat treated condition and are consistent with results of studies presented in this report.

Optical and scanning electron microscopy (SEM) images of S17-4 in a stress-relieved heat-treated condition are shown in Fig. 15 [51]. At higher magnification Fig. 15B shows a cellular solidification microstructure with columnar spacing in a sub-micrometer range. This is due to the rapid solidification of the melt pool [55]. XRD- analysis was conducted to estimate the volume fraction of FCC austenite and BCC ferrite-martensite. The three steel phases of BCC δ -ferrite, BCC α -ferrite, and BCC martensite have a very small difference in their tetragonality (see Fig. 1 and Fig. 4), and therefore not distinguishable with the available equipment for the XRD analysis. As previously mentioned, the amount of γ -austenite remained consistently between about 40 % and 50 % regardless of either the “as-manufactured” or stress-relieved condition.

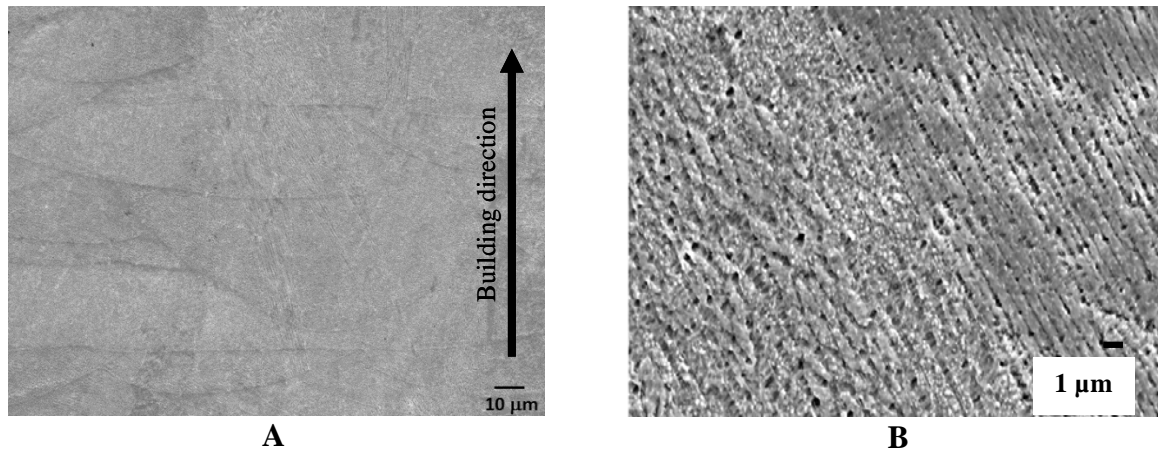


Fig. 15. Microstructure of AM S17-4 steel using the virgin powder along the build direction at low magnification (A), and high magnification (B) [51].

Similar observations of the microstructure of LPBF manufactured Cr-Ni steel alloys were made by other researchers [27, 38, 54, 56, 57]. As mentioned earlier, rapid cooling corresponds to smaller grain sizes and fine columnar spacing, which effect the amount of retained austenite in AM manufactured Cr-Ni stainless steels even after a stress-relief heat treatment. Reference [27] investigated the effect of different process gas atmospheres, either in the powder production and/or during the laser based PBF process, on the microstructure of S17-4. The non-heat treated “as-manufactured” S17-4 material was martensitic when the nitrogen or argon gas atomized S17-4 powder was processed in an argon atmosphere. If the S17-4 was manufactured in a nitrogen atmosphere, then different amounts of austenite were obtained depending on the powder atomization atmosphere. If the powder was nitrogen atomized the solidified S17-4 showed predominant FCC γ -phases. Results of their hardness measurements (HRC \approx 21) indicated predominant γ -phases even after the post heat treatment at a temperature of 482 °C for 1 hour. As a comparison, the hardness of the S17-4 using argon gas atomized powder and fabricated in argon environment was about HRC 30.

Reference [38] conducted experiments with nitrogen gas atomized S17-4 powder fabricating samples in nitrogen environment. They observed very fine, parallel, cylindrical metastable austenite grains in the “as-manufactured” non-post heat treated S17-4. The maximum amount of γ -phase was determined as 99.3 % in the “as-manufactured”, non-post heat treated S17-4 material and a nitrogen content of 0.17 mass % was detected. A post stress-relief heat treatment at a temperature of 650 °C for 1 hour did not affect the retained austenite and hence, the amount of martensite stayed constant at 0.7 %. However, the amount of martensite increased from 0.7 % to 3.7 %, when the same nitrogen atomized powder was processed in an argon environment [38]. The authors concluded that the very fine elongated grain structure occurred due to the rapid cooling and explained the existence of the metastable γ -phase in the LPBF manufactured S17-4 stainless steel and its high resistance to transform into martensite.

Reference [54] presented similar results for the obtained amounts of martensite and austenite, whether the S17-4 powder was either gas atomized in an Ar or N₂ atmosphere. They detected a nitrogen content of 0.15 mass % if the S17-4 powder was nitrogen gas atomized. Figure 17 shows the microstructure is characterized by columnar grains oriented in different directions. Phase analysis carried out by XRD determined approximately 75 % austenitic phases on the specimen

surface perpendicular to the building direction (vertical plane) and approximately 50 % on the specimen surface parallel to the building direction (horizontal plane) [54]. The result of an even co-existence of both martensitic and austenitic phases in S17-4 produced in a nitrogen environment is consistent with the XRD results presented by Ref. [51].

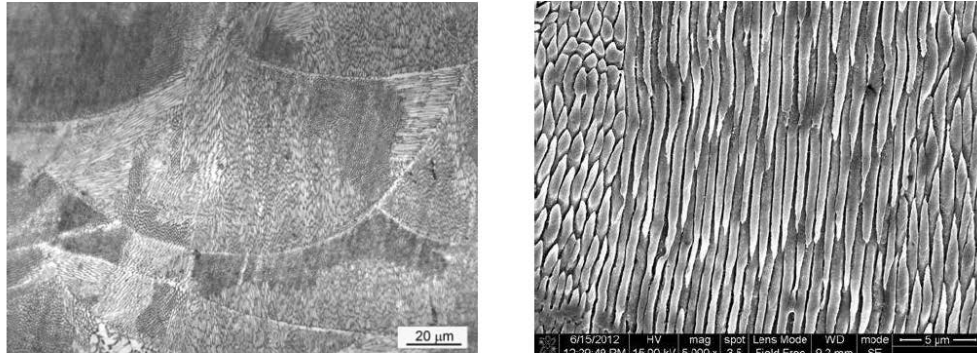


Fig. 16. Microstructure of S17-4 produced by LPBF, optical microscopy (left) and SEM (right) show strongly oriented, fine γ - grains [38].

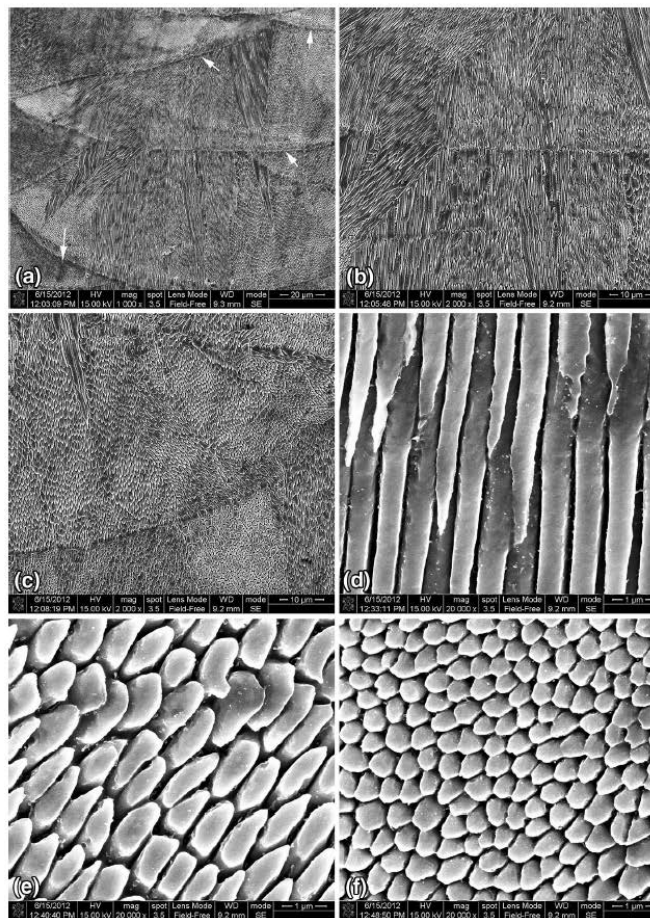


Fig. 17. SEM images (cross section view) of S17-4 manufactured by LPBF, a) overview, b) and c) magnified images from a, d) columnar grains parallel to building direction, e) columnar grain inclined to building direction, and f) columnar grain perpendicular to building direction, [54].

Further investigations of the effect of different process parameters on the microstructure of S17-4 processed by LPBF, with varying laser power (PL) and scan velocity (v_L) were made by Ref. [46]. The manufactured specimens were examined by optical microscopy and SEM in the directions parallel (YZ- plane) and perpendicular (XY- plane) to the building direction as presented in Fig. 18. The parameter combinations of PL and v_L in W and mm/s, respectively, are labeled in the upper right corner of the images in Fig. 18. The authors observed that the columnar grains showed a strongly preferred orientation since they nucleated along the heat transfer directions in both XY and YZ planes. Figure 18c shows the cross section through the grains indicating average diameter of the columnar austenite grains below 1 μm . The same study also stated that independent of the build parameters, approximately 70 % of martensite was observed along the build direction. This result is inconsistent with those results from Ref. [54], who have observed an amount of approximately 75 % austenite in the build direction.

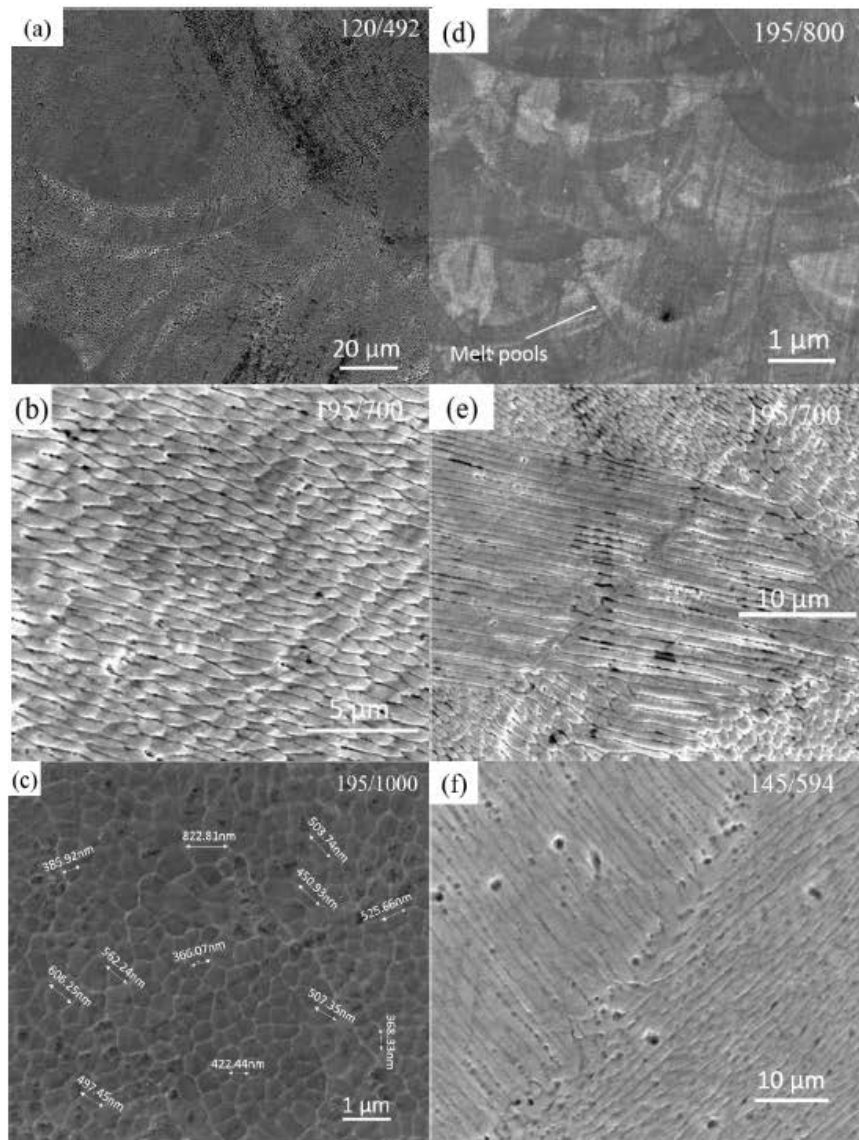
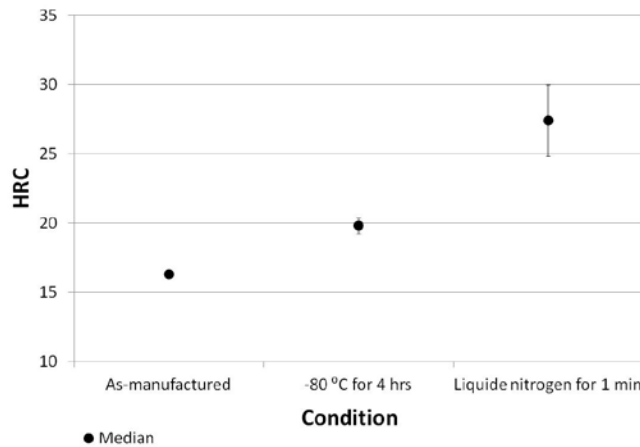


Fig. 18. SEM images in XY (a, b, and c) and YZ (d, e, and f) planes of S17-4 manufactured with various process parameters, [46].

The effects of scan velocity on the γ -grain sizes in a LPBF manufactured S17-4 are similar to the previously described results of laser-treated Cr-Ni stainless steel alloy by Ref. [19]. Apparently, similar thermal conditions occur during the LPBF process, as in the laser- and TIG welding of Cr-Ni steel alloys, which lead to similar thermal kinematics of forming a material microstructure characterized by fine dendritic and columnar grains of metastable γ -austenite and δ -ferrite along the γ -phase boundaries (see Fig. 6).

As previously mentioned, the fine grain structure of PBF manufactured metals is a result of the rapid cooling during the PBF build process. The isotherm TTT Diagram in Fig. 7 shows the expected steel phases of the martensitic steel, depending on how long it is treated in a certain temperature. The high cooling rates ($\approx 10^2$ °C / s) of the solidified S17-4 are so fast that potentially little to no solid state material diffusion will occur, which is necessary for the γ -austenite to decompose into α' -martensite.

Figure 19 shows the results of HRC measurements on two different sub-zero treated and the “as-manufactured” S17-4 stainless steel specimens. The values reported are the means of all hardness measurement indentations, except the first, made on samples treated at the stated conditions. The S17-4 stainless steel which was treated in liquid N₂ for only one minute shows an approximately 68 % increase of HRC compared to the non-treated, “as-manufactured” S17-4 stainless steel. In contrast, while the hardness of the cryogenically treated specimens in a freezer at -80 °C for four hours had less variation, the treatment achieved a lower increase in hardness (approximately 21 %) compared to the “as-manufactured” condition. The results indicate a hardening effect was possibly caused by an increasing fraction of a martensitic microstructure in the S17-4 material during the post-treatment. These results also support the hypothesis that temperatures as low as -154 °C are required to transform a significant amount of the retained metastable γ -austenite in an additively manufactured S17-4 material, assuming a nitrogen content of 0.15 mass %.



Specimen condition	HRC	
	Median	Standard deviation
“As manufactured”	16.3	0.304
Held at -80 °C in a freezer for 4 hrs	19.8	0.593
Submerged liquid nitrogen for 1 min	27.4	2.582

Fig. 19. Results of hardness measurement (HRC scale) for S17-4 in three different conditions, error bars are one standard deviation.

Increased hardness of S17-4 LPBF samples has also been observed after high-temperature post-processing. For instance, Ref. [51] studied the effect of a stress relief heat treatment at a temperature of 650 °C, held for one hour, and slow cooling inside the furnace. The measured hardness of the “as-manufactured” S17-4 (between 16 HRC and 18 HRC) is similar to values found in the current study for the “as-manufactured” samples and those held at a temperature of -80 °C for 4 hours. The lower hardness values in that earlier work were attributed to the existence of austenite, which dominates after the LPBF process and is softer than martensite. After the high-temperature stress relief, the hardness increased by approximately 50 % (between 23 HRC and 25 HRC), which is similar to, but slightly below the hardness of the treated specimens in the current study that were treated by submersion liquid N₂. Reference [51] attributed the increased hardness due to the high-temperature heat treatment to changes in microstructure, resulting from the specific stress relief heat treatment procedure. The long duration at high temperatures possibly allowed carbides and other intermediate phases to form in addition to the martensitic transformation [6]. However, their results of XRD measurements did not show any significant martensitic transformation and the amount of FCC austenite remained consistently between about 40 % and 50 % regardless of either the “as-manufactured” or stress-relieved condition [51].

Comparing the hardness values reported by Ref. [27] with those shown in Fig. 19, it can be concluded that the cryogenic treatment in liquid N₂ at temperatures about -196 °C for one minute caused a significant amount of metastable retained γ -austenite to decompose into martensite and incoherent carbides, e.g., Fe₃C, resulting in an increase of hardness from 16.3 HRC up to 27.4 HRC (see Fig. 19).

5. Conclusions

The objective of this study was to predict the effects of the chemical composition in Cr-Ni stainless steel alloys on their material microstructure, manufactured in a LPBF process. Two stainless steel alloys, S17-4 and S15-5, were chosen to calculate the values for the chromium- and modified nickel equivalent (Eqs. (2) and (5)) and inscribed these values into the Schöffler and DeLong diagrams (see Fig. 9, Fig. 10, and Fig. 11). This work showed that the prediction of the material phases is strongly affected by the production history of the stainless steel powder, e.g., gas atmosphere during the atomization and the build environment in the LPBF process. The amount of α -ferrite, stable and metastable retained γ -austenite, δ -ferrite, martensite, and carbides in Fe-Cr-Ni alloys depends on their chemical composition, those weight fractions, and on the thermal conditions during the solidification. The predicted stainless steel phases in a LPBF manufactured S17-4 obtained by the Schöffler diagram were compared with results from other previous research about the observed material microstructure and mechanical properties [27, 46, 51, 53, 54, and 56]. All these studies agree that in additively manufactured S17-4 stainless steel, built in a nitrogen environment and using nitrogen atomized powder, a primary austenitic solidification occurs and phases of metastable retained γ -austenite, martensite, and δ -ferrite can coexist. Results of the XRD analysis presented by Ref. [51] and Ref. [54] showed volume fractions of FCC austenite consistent between about 50 % to 55 % in a “as-manufactured” condition. The presence of such a high volume fraction of retained γ -austenite is most likely from a rapid cooling, i.e., quenching from above the austenite transformation temperature or from above the upper critical martensite starting temperature. The coexistence of metastable γ -austenite, martensite, and incoherent Fe₃C in a nitrogen environment built S17-4 may be explained by the thermal condition during the LPBF process. It is assumed that the decomposition of the primarily solidified metastable γ -austenite into martensite and Fe₃C is due to a self-aging effect by the next melted and solidified layers during

the LPBF process. The roughly equal volume fraction of FCC austenite and BCT martensite changed not significantly after a stress relief heat treatment at a temperature of 650 °C [51]. This indicates a strong stability of the retained γ -austenite phases in the “as-manufactured” S17-4 material, which can be predicted by the calculation of the M_{d30} temperature under consideration of the sub-micrometer sizes of the columnar γ -austenite grains. A grain size refinement leads to a decrease either of the M_S and M_F temperatures. A similar effect was shown on AISI 420 stainless steel surface treated by a laser. Reference [43] showed a decrease of M_S to room temperature of 20 °C for grain sizes smaller than 10 μm after the surface was treated by the laser. Temperatures as low as -154 °C are required to continue the austenite to martensite transformation in a LPBF manufactured S17-4 stainless steel with an assumed nitrogen content of 0.15 mass %. Results from the hardness measurements showed a significant increase of hardness up to \approx HRC 30 after the S17-4 was cryogenically treated in submerged liquid nitrogen at temperatures below the previously calculated M_{d30} temperature of -154 °C. This indicated a predominately martensitic microstructure after the cryogenic treatment and these results are consistent with previous results [27]. A predominantly martensitic microstructure was observed in an Ar environment built S17-4 (\approx HRC 30). Results from tensile tests [51] and from ferritoscope measurements [38] show that the gradually increasing degree of the cold working defines the transformation from metastable austenite into an increasing amount of martensite [38]. It seems that the Schöffler and the DeLong Diagrams are helpful tools to predict the obtained steel phases in additively manufactured Cr-Ni stainless steels. In conclusion of the observed phase transformation, it seems that LPBF manufactured S17-4 is effectively in a solution-treated condition.

Acknowledgments

I would like to acknowledge the contributions from my group leader, Dr. Alkan Donmez. Without his thoughtful review and suggestions for improvements, this work would not have been possible. I would like to thank him for the excellent cooperation during the writing process and for editing of this document. I also would like to thank him for the opportunity to be a member of his research group for additive manufacturing at the National Institute of Standard and Technology (NIST), Gaithersburg, USA, during the last four years. I am grateful to Mr. Carlos R. Beauchamp for performing the hardness measurements and to Dr. Jarred Heigel for his thoughtful review.

References

- [1] ASTM A564 / ASTM A564M (2013) *Standard Specification for Hot-Rolled and Cold-Finished Age-Hardening Stainless Steel Bars and Shapes*, ASTM International, West Conshohocken, PA.
- [2] Schäffler, A. L. (1949) Constitution diagram for stainless steel weld metal. *Metal Progress, Volume 56, Issue 11: page 680 and 680B*.
- [3] DeLong, W. T. (1974) Ferrite in austenitic stainless steel weld metal, *Welding Journal, Volume 53, Issue 7, pp: 273 to 286*
- [4] Bautsch, H. J., Bohm, J., and Kleber, H. (1998) *Einfuehrung in die Kristallografie, Oldenbourg Wissenschaftsverlag GmbH Muenchen, Germany*.
- [5] Zimmermann, R. and Guenther, K. (1975) *Metallurgie und Werkstofftechnik, Ein Wissensspeicher – Band 1, Leipzig, Germany, Deutscher Verlag der Grundstoffindustrie*
- [6] Seidel, W. (2001) *Werkstofftechnik, Werkstoffe – Eigenschaften – Preufung – Anwendung, 5. Auflage, Carl Hanser Verlag, München, Germany*.
- [7] Schatt, W. (1981) *Werkstoffe des Maschinen-, Anlagen- und Apperatebaus, VEB Deutscher Verlag fuer Grundstoffindustrie, Leipzig, Germany, 2 Auflage*.
- [8] Schumann, H., Oettel, H. (2005) *Metallography, Wiley-VCH, Weinheim, p.665*
- [9] Eckstein, H.J. (1971) *Waermebehandlung von Stahl – Metallkundliche Grundlagen, Leipzig, Germany, Verlag fuer Grundstoffindustrie*.
- [10] Liedke, D. (2005) *Merkblatt 450 – Waermebehandlung von Stahl, Haerten, Anlassen, Vergueten, Bainitisieren, Duesseldorf, Germany, Stahl-Informations-Zentrum*.
- [11] Manna, R. (2016) *Temperature Time Transformation Diagram, Center of Advanced Study, Department of Metallurgy Engineering Institute of Technology, Banaras*

Hindu University, Varanasi-221 005, India,
http://digital.csic.es/bitstream/10261/78356/4/41_ISIJ_capdevila.pdf p. 76.

- [12] Bhaduri, A. K., Sujith, S., Srinivasan, G., Gill, T. P. S., and Mannan, S. L. (1995) Optimized Postweld Heat Treatment Procedures for 17-4 PH Stainless Steels, *Welding Research Supplement I*, pp. 153-159.
- [13] EOS mill test certificate, MTC, S17-4PH, F491201 GP1, (2013) *EOS Finland*.
- [14] EOS mill test certificate, MTC, S15-5, J451301, PH1, (2013) *EOS Finland*.
- [15] ThyssenKrupp, material specification for 1.4542 (17-4PH), (2017) pdf- file from company's homepage: http://www.thyssenkrupp.ch/documents/rsh_stab_4542.pdf.
- [16] Schulze, G. (2009) Die Metallurgie des Schweissens, *Heidelberg-Dordrecht-London-New York: Springer Verlage*.
- [17] Bobadilla, M., Lacaze, J., and Lesoult, G.(1988) Influence des conditions de solidification sur le déroulement de la solidification des aciers inoxydables austénitiques, *Journal Crystal Growth, Volume 89*, pp. 531-544.
- [18] Fukumoto, S. and Kurz, W (1997) The δ to γ Transition in Fe-Cr-Ni Alloys during Laser Treatment, *The Iron and Steel Institute International Japan, Volume 37, Number 7*, pp. 677-684.
- [19] Fukumoto, S. and Kurz, W (1998) Prediction of the δ to γ Transition in Austenitic Stainless Steels during Laser Treatment, , *The Iron and Steel Institute International Japan, Volume 38, Number 1*, pp. 71-77.
- [20] Mizukami, H., Suzuki, T., and Umeda, T. (1993) Initial stage of rapid solidification of 18-8 stainless steel, *Materials Science and Engineering, Volume 173, Issues 1–2*, pp 361-364.
- [21] Koseki, T. and Flemings, M.C. (1997) Solidification of undercooled Fe-Cr-Ni alloys: Part III. Phase selection in chill casting, *Metallurgical and Materials Transactions, Volume 28A, Issue 11*, pp 2385–2395.
- [22] Volkmann, T.; Herlach, D.M, and Löser, W. (1997) Nucleation and phase selection in undercooled Fe-Cr-Ni melts: Part I. Theoretical analysis of nucleation behavior, *Metallurgical and Materials Transactions A, Volume 28, Issue 2*, pp 453–460.
- [23] Nakao, Y., Nishimoto, K., and Zhang, W. (1998) Analysis of isothermal solidification process on transient liquid insert metal diffusion bonding, *Journal Japan Welding Society, Volume 7*, page 414.
- [24] Kurz, W., Giovanola, B, and Trivedi, R. (1986) Theory of microstructural development during rapid solidification, *Acta Metallurgica, Volume 34, Issue 5*, pp. 823-830.

- [25] Fukumoto, S. and Kurz, W. (1999) Solidification Phase and Microstructure Selection Maps for Fe-Cr-Ni Alloys, *The Iron and Steel Institute International Japan, Volume 39, Number 12, pp. 1270-1279.*
- [26] ASTM E8/E8M (2013) Standard Test Methods for Tension Testing of Metallic Materials, *ASTM International, West Conshohocken, PA.*
- [27] Murr, L.E., Martinez, E., Hernandez, J., Collins, S., Amato, K.N., Gaytan, S. M., and Shindo, P. W. (2012) Microstructure and Properties of 17-4 PH Stainless Steel Fabrication by Selective Laser Melting, *Journal of Materials Research and Technology, Volume 1, Issue 3, pp. 167-177.*
- [28] Wever, F., Peter, W, and Rose, A.; Atlas zur Waermebehandlung der Staehle, *Verlag Stahleisen mbH, Duesseldorf, West Germany, 1954/56/58, Vol. 1, Strassburg W., Rademacher L., Vol. 2.*
- [29] Edelstahl, Merkblatt 827, 2016,
http://www.edelstahl-rostfrei.de/downloads/iser/MB_827.pdf
- [30] ASM Specialty Handbook Stainless Steels, Metallurgy and Properties of Wrought Stainless Steels, *ASM International Materials Park, OH 1994, p. 13.*
- [31] Krauss G. (2005) Steel: Processing, Structure, and Performance, *ASM International, Metals Park, Ohio, USA.*
- [32] Hull, F. C (1960) Effects of Alloying Additions on Hot Cracking of Austenitic Chromium-Nickel Stainless Steels, Proceedings, *American Society for Testing and Materials, Volume 60, pp. 667 to 690.*
- [33] Castro, R.J. and J.J. de Cadenet (1975) Welding metallurgy of stainless and heat resisting steels, *Cambridge University Press, ISBN: 0 521 20431 3.*
- [34] Potak, M., Sagalevich, E.A. (1972) Structural diagram of stainless steels as applied to cast and metal deposited during welding, *Avt. Svarka, Volume 5, pp. 10 to 13.*
- [35] Ferree, Jr., J. A. (1969) Free Machining Austenitic Stainless Steel, *U.S. Patent 3-460, 939.*
- [36] Kotecki, D.J. and Hilkes, J. (1994) Welding Process for Duplex Stainless steels, , *Weldability of Materials Proceedings of the Materials Symposium, ASM International, Materials Park.*
- [37] Kotecki, D. J. and Siewert T.A (1992) WRC-1992 Constitution Diagram for stainless steel weld metals: A modification of the WRC-1988 Diagram, *Welding Journal, Volume 71, Issue 5, pp. 171-178.*

- [38] Starr, T. L., Rafi, K. H., Stucker, B. E., and Scherzer, C. M. (2012) Controlling Phase Composition in Selective Laser Melted Stainless Steels, *International Solid Freeform Fabrication Symposium, University of Texas, Austin*, pp. 439-446.
- [39] Abrassart, F. Stress-induced $\gamma \rightarrow \alpha$ martensitic transformation in two carbon stainless steels. Application to trip steels, 1970 – 2016, *Metallurgical and Materials Transactions B, Volume 47B, ISSN: 1073-5615 (Print)*, pp. 1543-1916.
- [40] Rajan, B., Roychowdhury, S., Vivekanand, K., and Raja, V.S. (2013) Effect of Reverted Austenite on Mechanical Properties of Precipitation Hardenable 17-4 Stainless Steel, *Material Science Engineer, Volume 568A*, pp 127–133.
- [41] Zhang, S. and Findley, K.O. (2013) Quantitative Assessment of the Effects of Microstructure on the Stability of Retained Austenite in TRIP Steels, *Acta Materials, Volume 61, Issue 6*, p 1895–1903.
- [42] Takaki, S., Fukunaga, K., Syarif, J., and Tsuchiyama, T. (2004) Effect of Grain Refinement on Thermal Stability of Metastable Austenitic Steel, *Material Transactions, Volume 45, Issue 7*, pp 2245–2251.
- [43] Colaço, R. and Vilar, R. (2004) Stabilisation of retained austenite in laser surface melted tool steels, *Materials Science and Engineering, Volume 385A, Issues 1–2*, pp 123–127.
- [44] Nohara, K., Ono, Y. Ohashi, N. (1977) Composition and grain size dependencies of strain-induced martensitic transformation in metastable austenitic stainless steels., *Journal of the Iron and Steel Institute of Japan, Volume 63, Issue 5*, pp 212 – 222.
- [45] ASTM E112 (2012) Standard Test Methods for Determining Average Grain Size, , *ASTM International, West Conshohocken, PA*.
- [46] Gu, H., Gong, H., Pal, D., Rafi, K., Starr, T., and Stucker, B. (2013) Influences of Energy Density on Porosity and Microstructure of Selective Laser Melted 17-4PH Stainless Steel, *International Solid Freeform Fabrication Symposium, University of Texas, Austin*, pp 474-489.
- [47] Wu, R., Wei, L., Zhou, S., Zhong, Y, Wang, Li, and Jin, X. (2014) Effect of Retained Austenite on the Fracture Toughness of Quenching and Partitioning (Q&P)-Treated Sheet Steels, *Metallurgical and Materials Transactions, Volume 45A, Issue 4*, pp 1892–1902.
- [48] Das, D., Dutta, A.K., and Ray, K.K. (2010) Sub-zero Treatments of AISI, D2 steel, Part I. Microstructure and Hardness, *Material Science Engineering A*, 527, pp. 2182-2193, DOI: 10.1016/j.msea.2009.10.070.
- [49] Jacob, G., Donmez, A., Slotwinski, J., Moylan, S. (2016) Measurement of powder bed density in powder bed fusion additive manufacturing processes, *Measurement Science and Technology, 104002.R1. Thomas Reuters*.

- [50] ASTM E18 (2016) Standard Test Methods for Rockwell Hardness of Metallic Materials 1, 2, , *ASTM International, WEST Conshohocken, PA.*
- [51] Jacob, G., Brown, C., Donmez, A., Watson, S., and Slotwinski, J (2017) Effect of powder recycling on stainless steel powder and built material properties in metal powder bed fusion processes, *NIST- Advanced Manufacturing Series 100-6*, <https://doi.org/10.6028/NIST.AMS.100-6>.
- [52] Schumann, H. (1991) Metallographie, , *Stuttgart, Germany, Deutscher Verlag für Grundstoffindustrie.*
- [53] Kumpaty, S., Kamara, S., Tomlin, B., Yoo, J., Kumpaty, H., Anderson, D., Govindaraju, M., Kanoongo, N., and Balasubramanian, K. (2013) Effect of Heat Treatment on Mechanical/Metallurgical Properties of Direct Metal Laser Sintered 17-4 Precipitate Hardened Stainless Steel, *Advanced Material Research, ISS: 1662-8985, Vol. 699, pp 795-801*
- [54] Rafi, H.K, Pal, D., Patil, N. Starr, T. L., and Stucker, B. E. (2014) Microstructure and Mechanical Behavior of 17-4 Precipitation Hardenable Steel Produced by Selective Laser Melting, *Journal of Materials Engineering and Performance, Volume 23, pp. 4421 to 4428.*
- [55] Vilaro, T., Colin, C., and Bartout, J.D. (2011) As-Fabricated and Heat-Treated Microstructures of the Ti-6Al-4V Alloy Processed by Selective Laser Melting, *Metal Material Transformations, Volume 42A, pp.3190-3199.*
- [56] Khalid, H., Rafi, D., Pal, Patil, N., Starr, T. L., and Stucker, B. E. (2014) Microstructure and Mechanical Behavior of 17-4 Precipitation Hardenable Steel Processed by Selective Laser Melting , *Journal of Materials Engineering Performance, Vol. 23, 4421–4428.*
- [57] Murr, L.E., Martinez, E., Amato, K. N., Gaytan, S. M., Hernandez, J., Ramirez, D. A., Shindo, P.M., Medina, F., and Wicker, R. B. (2012) Fabrication of Metal and Alloy Components by Additive Manufacturing: Examples of 3D Materials Science, *Journal of Materials Research and Technology, Volume 1, pp. 42-45.*